Available online at www.sciencedirect.com
ScienceDirect
Journal of Volcanology and Geothermal Research 167 (2007) 212–238
Journal of volcanology and geothermal research
www.elsevier.com/locate/jvolgeores

Spatiotemporal evolution of a marine caldera-forming eruption, generating a low-aspect ratio pyroclastic flow, 7.3 ka, Kikai caldera, Japan: Implication from near-vent eruptive deposits

F. Maeno [a,b,*], H. Taniguchi [c]

[a] *Institute of Mineralogy, Petrology, and Economic Geology, Graduate School of Science, TOHOKU University, Aoba, Aoba-ku, Sendai, 980-8578, Japan*
[b] *Volcanic Research Center, Earthquake Research Institute, University of TOKYO, 1-1-1, Yayoi, Bunkyo-ku, Tokyo, Japan*
[c] *Center for Northeast Asian Studies, Tohoku University, Kawauchi, Aoba-ku, Sendai, Japan*

Received 24 January 2006; received in revised form 28 March 2007; accepted 11 May 2007
Available online 21 May 2007

Abstract

The VEI 7, 7.3 ka caldera-forming eruption of the Kikai caldera occurred in a shallow sea, and caused devastating damage to the prehistoric human settlements of southern Kyushu, Japan. This Holocene activity at this volcano records eruptions with compositional range of 56 to 74 wt.% in SiO_2 spanning with the climactic eruption. In this study, stratigraphy, component, and lithology of the pyroclastic deposits were analyzed at near-vent islands (Satsuma Iwo-jima and Take-shima) in order to reconstruct this eruption. Stratigraphic sections are characterized by plinian pumice-fall deposits (Unit A), intraplinian flow deposits (Unit B), climactic pyroclastic flow deposits (Units C1–C3), and co-ignimbrite ash-fall deposits (Unit D). In total the estimated magma volume in the system was 70–80 km^3 (DRE) and the eruption therefore represents the evacuation of a major silicic magmatic system. The plinian stage (Phase 1) is subdivided into an initial small phase and a second large one. The column height in the second phase was estimated to be 40–43 km. The total tephra volume of this stage was estimated to be 40 km^3. The magma discharge rate has been calculated from the column height data to be 2×10^8 kg/s. The eruption duration is also estimated to be a minimum of approximately 28 h. Collapse of the column (Phase 2) produced Unit B, which consists of multiple thin lithic-rich or pumice-rich layers or pods, including welded pumice-fall layers. The deposits are characterized by stratified or cross-stratified facies and display various degree of welding. These sedimentary characteristics indicate that, during the plinian column collapse, high temperature turbulent density currents were generated where dense pyroclasts were well segregated, resulting in the lithic-rich layers or pods. Phase 3 is characterized by Units C1–C3. Unit C1 shows non-welded stratified facies, which consist of lithic and crystals, including quenched juvenile materials as a minor constituent. Unit C2 displays welded stratified facies, which consist of lithic-rich layers and pumice-rich layers. These two subunits occur only in topographic lows in Satsuma Iwo-jima. Unit C3 is thickest and poorly-sorted non-welded massive deposit, which includes fragments of welded tuff from underlying units in proximal regions. These facts indicate that multiple pyroclastic density currents produced Units C1 and C2 in the near-vent area, and were followed by the main sustained current producing Unit C3, a low-aspect ratio ignimbrite, distributed over a wide area of southern Kyushu across the sea. Varying extents of magma–water interactions started during Phase 2, continuing during the early stages of Phase 3, and diminished during the climactic C3 ignimbrite stage. In addition, collapse of the caldera may have started before Unit C deposition, based on the evidence of a fault overlain by Unit C on the caldera rim. The collapse may have initiated water access to the magma. The

* Corresponding author. Volcano Research Center, Earthquake Research Institute, University of TOKYO, 1-1-1, Yayoi, Bunkyo-ku, Tokyo, Japan. Fax: +81 3 3812 6979.
E-mail address: fmaeno@eri.u-tokyo.ac.jp (F. Maeno).

0377-0273/$ - see front matter © 2007 Elsevier B.V. All rights reserved.
doi:10.1016/j.jvolgeores.2007.05.003

source appears to have been biased toward the western side of the caldera. The Holocene evolution of the Kikai volcano records the existence of a large silicic magma system at depths of about 7 km that coexisted with or was regularly recharged with mafic magma.
© 2007 Elsevier B.V. All rights reserved.

Keywords: marine caldera-forming eruption; low-aspect ratio ignimbrite; pyrocalstic density currents; Kikai caldera

1. Introduction

While most work on recent eruptions is focused on on-land events, many Quaternary caldera-forming eruptions have occurred in areas of shallow seas or lakes, with the production of voluminous pyroclastic flows (Cas and Wright, 1991; Fisher et al., 1993; Carey et al., 1996; Allen and Cas, 2001). Such eruptions are therefore a crucial part of the record of silicic magmatism. The 1883 eruption of Krakatau in Indonesia (Simkin and Fiske, 1983; Carey et al., 1996, 2000) and the 3.5 ka Minoan eruption of Santorini in Greece (Heiken and McCoy, 1984; McCoy and Heiken, 2000) are the most famous examples of recent marine caldera-forming eruptions. Other Quaternary marine silicic calderas have been also discovered on subduction zones and near ocean islands; the Shichito–Iwo-jima Ridge, Izu–Ogasawara (or Izu–Bonin) Arc (Yuasa et al., 1991), the Kermadec Ridge north of Taupo volcanic zone, New Zealand (Wright and Gamble, 1999), and the Hellenic Island Arc in Greece (Allen and Cas, 1998). Although these eruptions must have significantly and devastatingly affected the development of coastal human activities and environments around the volcanoes, they still remain speculative and controversial, especially with respect to the effects of seawater on dynamics and evolution of such large-scale silicic marine eruptions. The reasons for this include the rare occurrence and violent nature of this type of eruption, the lack of direct observations, and difficulties arising from global variations in sea levels and local tectonic or volcano-tectonic effects (e.g. Allen and Cas, 1998).

The 7.3 ka eruption at Kikai volcano, Japan, occurred in a shallow sea. The volcanic explosivity index (VEI; Newhall and Self, 1982) is 7, based on total volume of products (150–170 km^3; Machida and Arai, 2003), which was larger in scale than the celebrated Santorini and Krakatau eruptions (VEI is 6), and this eruption was the largest in the last 10 ka in Japan. Previous researchers (Ui, 1973; Ono et al., 1982; Walker et al., 1984) characterized a major sequence of the deposits in the 7.3 ka Kikai eruption. They showed that the eruption produced plinian fallout, followed by intraplinian flows, and a climactic pyroclastic flow as a low-aspect ratio ignimbrite (Walker et al., 1980), that traveled over the sea and resulted in devastating damage to prehistoric human activities in southern Kyushu. However, they did not carry out a precise analysis of the lithofacies in the eruptive deposits, especially in the near-vent area, and did not discuss the evolution of this eruption in detail. In this paper, the 7.3 ka caldera-forming eruption of Kikai volcano is reconstructed based on analyses of the stratigraphy, textural, and lithofacies characteristics, and components of the pyroclastic deposits (mainly in proximal areas), which are useful qualitative indicators of the temporal evolution of the eruption intensity and the relative timing of the onset of the catastrophic caldera collapse. Such studies can provide constraints on predicted patterns for future explosive activity, and are an important part of ongoing studies of the hazards of marine silicic eruptions.

2. Geological setting and background

Kikai Caldera, 17 km wide and 20 km long, is a Quaternary volcano located in the East China Sea, southern Kyushu. The caldera is located in the southern extension of the Kagoshima graben, which is a trough-shaped volcano-tectonic depression 30 km wide and 120 km long that trends NNE–SSW across the southernmost part of Kyushu Island (Fig. 1). Most of the Kikai caldera is now 300–500 m beneath the sea. The subaerial parts are two islands, Take-shima and Satsuma Iwo-jima, representing subaerial parts of the northern caldera rim (Fig. 2). Iwo-dake (rhyolitic volcano) and Inamura-dake (basaltic volcano) on Satsuma Iwo-jima are the tops of the submerged post-caldera stratovolcanoes under the sea (Ono et al., 1982). In the Kikai caldera, multiple caldera-forming eruptions have occurred within the latest a few hundreds of thousand years. Deposits from these eruptions are distributed on islands in and around the Kikai caldera.

On the outer flanks of the caldera wall of the two islands of Kikai caldera, three sheets of ignimbrite are exposed; the 140 ka Koabi ignimbrite (Ono et al., 1982; Machida et al., 2001), the 95 ka Nagase ignimbrite (Ono

Fig. 1. Geomorphological map of Southern Kyushu and Kikai caldera, southern extension of the Kagoshima Volcano-tectonic graben. Location numbers are also shown, 19 (Ei) in Satsuma Peninsula and 20 (Izashiki) in Osumi Peninsula.

et al., 1982), and the latest 7.3 ka Koya–Take-shima ignimbrite (Ui, 1973; Ono et al., 1982). On both of Satsuma Iwo-jima and Take-shima, the Komorikô tephra group (13 to 8 ka) is also exposed (Okuno et al., 2000). Inside the caldera wall on the Satsuma Iwo-jima, there are post-7.3 ka rhyolitic and basaltic lavas

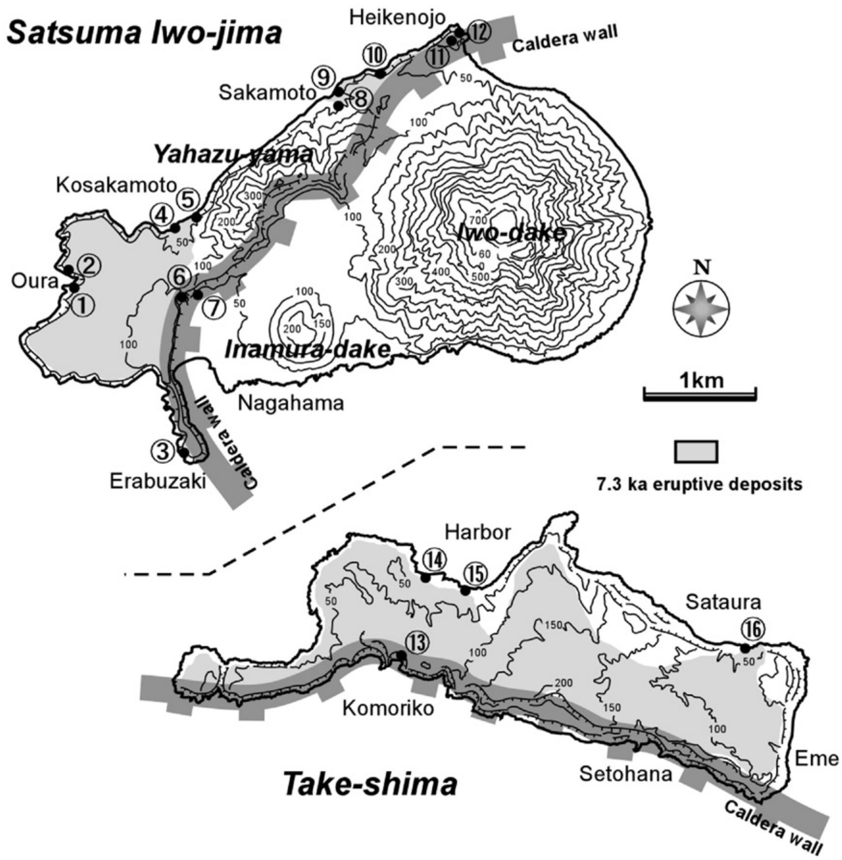

Fig. 2. Distribution of the 7.3 ka eruptive deposits in Satsuma Iwo-jima and Take-shima (shaded area), and outcrop distribution (location numbers: 1–16).

and tephras, that erupted from the Iwo-dake and Inamura-dake volcanoes after the 7.3 ka eruption (Ono et al., 1982; Kawanabe and Saito, 2002; Maeno and Taniguchi, 2005). In 1934–1935, a new silicic lava dome, Showa Iwo-jima Island, was produced from a submarine eruption, which is the latest magmatic eruption in the Kikai caldera (Tanakadate, 1935; Maeno and Taniguchi, 2006).

The 7.3 ka eruption produced four major units, which can be observed on some proximal islands (notably Satsuma Iwo-jima and Take-shima islands) around the Kikai caldera (Fig. 2) and on the mainland of Kyushu. The lowermost unit consists of plinian pumice-fall deposits. This has been named 'the Koya pumice fallout' by Ui (1973) for the distal mainland Kyushu, or 'the Funakura pumice fallout' by Ono et al. (1982) and Walker et al. (1984) for the proximal islands. Next comes the intraplinian flows, which deposited only proximal areas (the Funakura pyroclastic flow; Ono et al., 1982; Walker et al., 1984; Kobayashi and Hayakawa, 1984). The third unit is a voluminous ignimbrite, which has been named 'the Koya ignimbrite' by Ui (1973) for the distal area, or 'the Take-shima ignimbrite' by Ono et al. (1982) and Walker et al. (1984) for the proximal islands. This ignimbrite is traceable up to 100 km away from the source and has been interpreted as a low-aspect ratio ignimbrite by Walker et al. (1980, 1984) and Ui et al. (1984). The topmost unit on the mainland Kyushu is co-ignimbrite ash-fall deposit, named 'the Akahoya Ash' by Machida and Arai (1978). This tephra was dispersed over a wide area of Japan, more than 1000 km far away from the Kikai caldera, and the total volume has been estimated to be about 100 km^3 (Machida and Arai, 1978, 2003). Since sea level reached its highest with the warming climate around 7 to 6.5 ka, it has remained relatively unchanged, fluctuating several times within an amplitude of 2–3 m (Zheng et al., 1994; Ōki, 2002).

3. Stratigraphy of the 7.3 ka eruptive deposits

Pyroclastic deposits found in proximal areas have been interpreted as time slices representing the evolution of the 7.3 ka caldera-forming eruption. In proximal areas, the 7.3 ka eruptive deposits exposed on the two islands

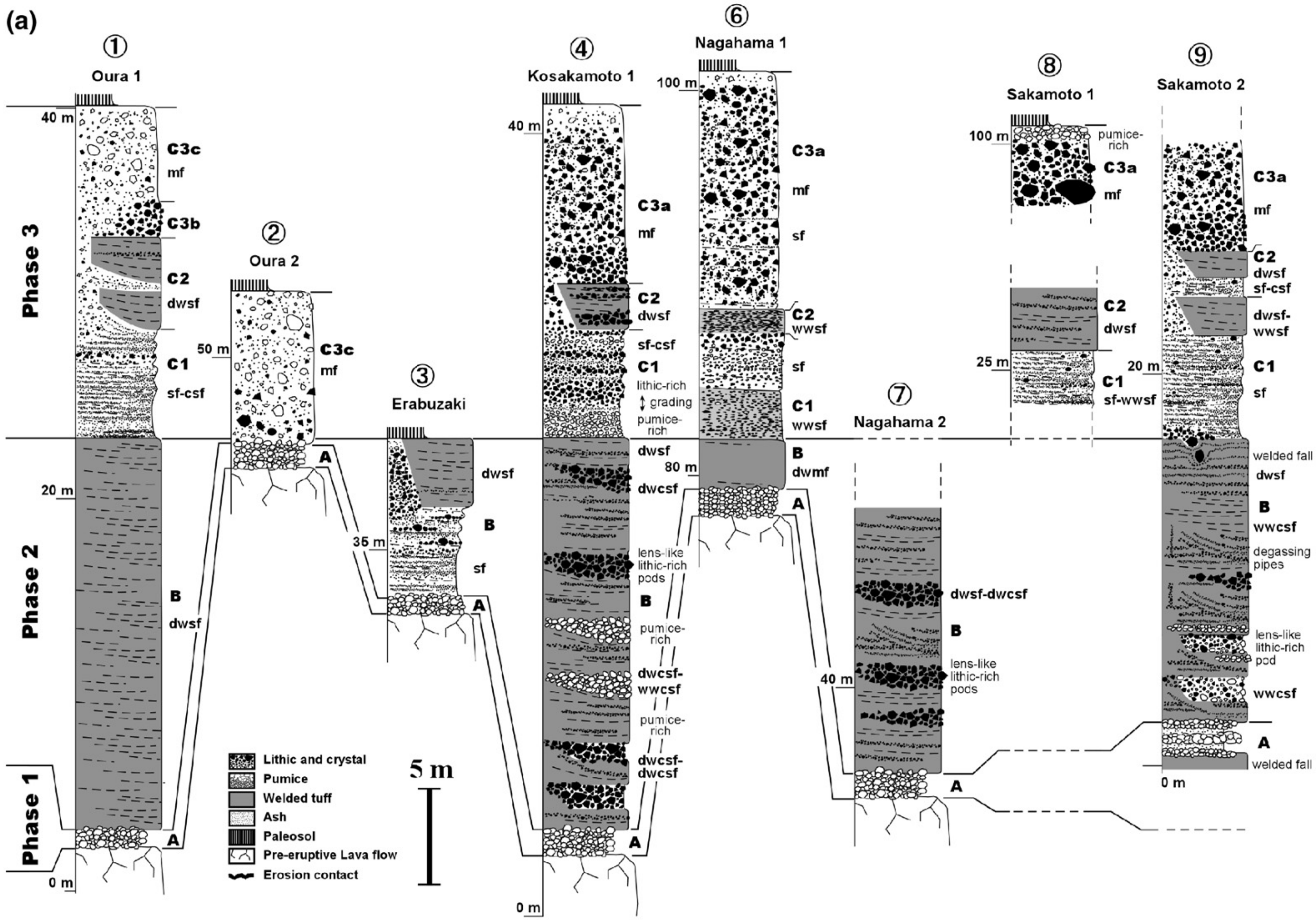

Fig. 3. (a and b) Representative stratigraphic columns through the 7.3 ka eruptive deposits in Satsuma Iwo-jima (locations 1–12), Take-shima (13–16), Satsuma Peninsula (19), and Osumi Peninsula (20). Deposits are divided into three main units (Units A–C). mf: non-welded massive facies, wwmf: weakly welded massive facies, dwmf: densely welded massive facies, sf: non-welded stratified facies, wwsf: weakly welded stratified facies, dwsf: densely welded stratified facies, csf: cross-stratified facies, wwcsf: weakly welded cross-stratified facies, dwcsf: densely welded cross-stratified facies. Units A and C are subdivided into four and three subunits, respectively. (c) Detailed columns through Unit A pumice fall deposits (from A1 to A4) in Satsuma Iwo-jima (locations 2–12) and Take-shima (locations 13–16).

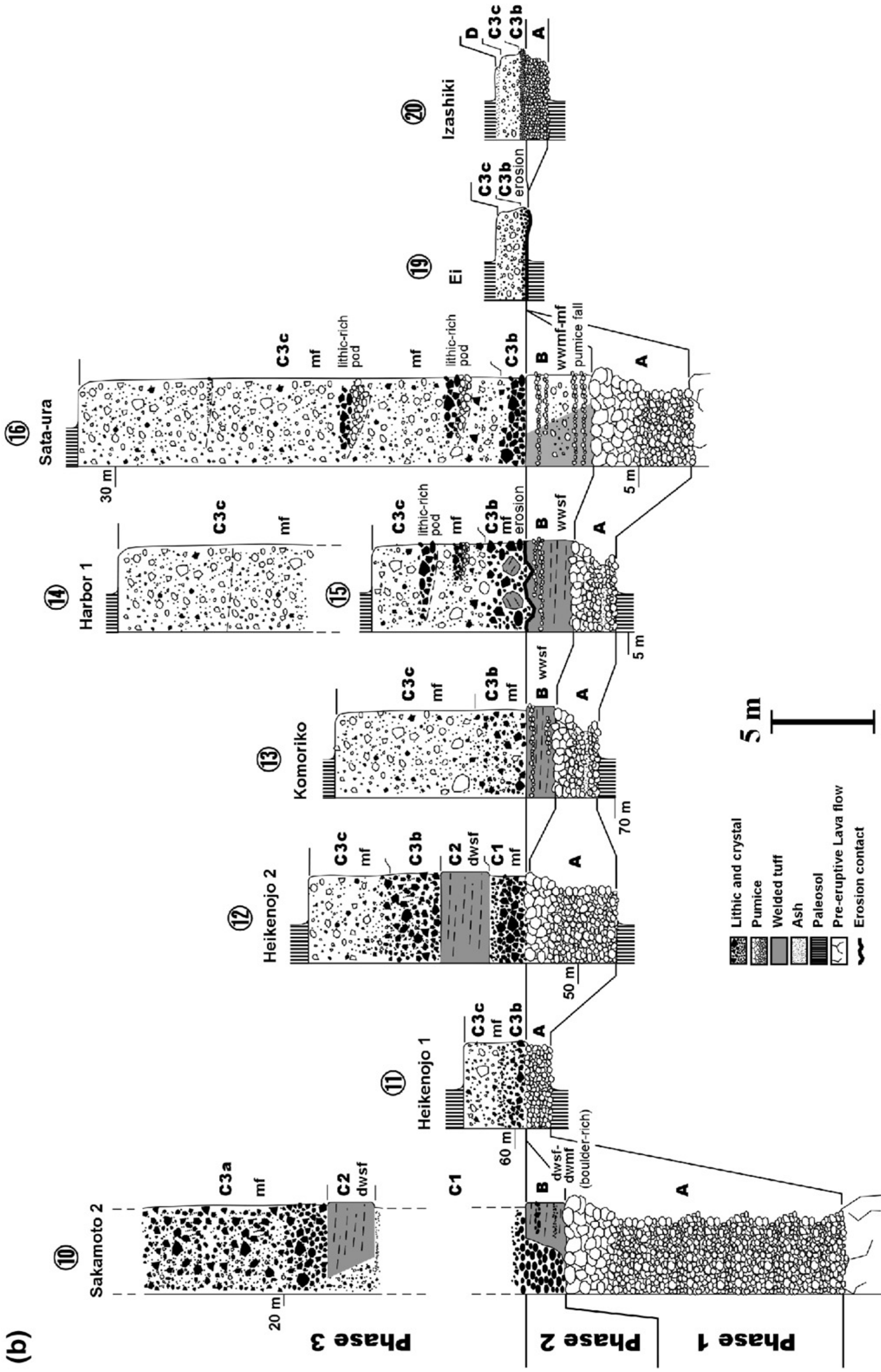

Fig. 3 (*continued*).

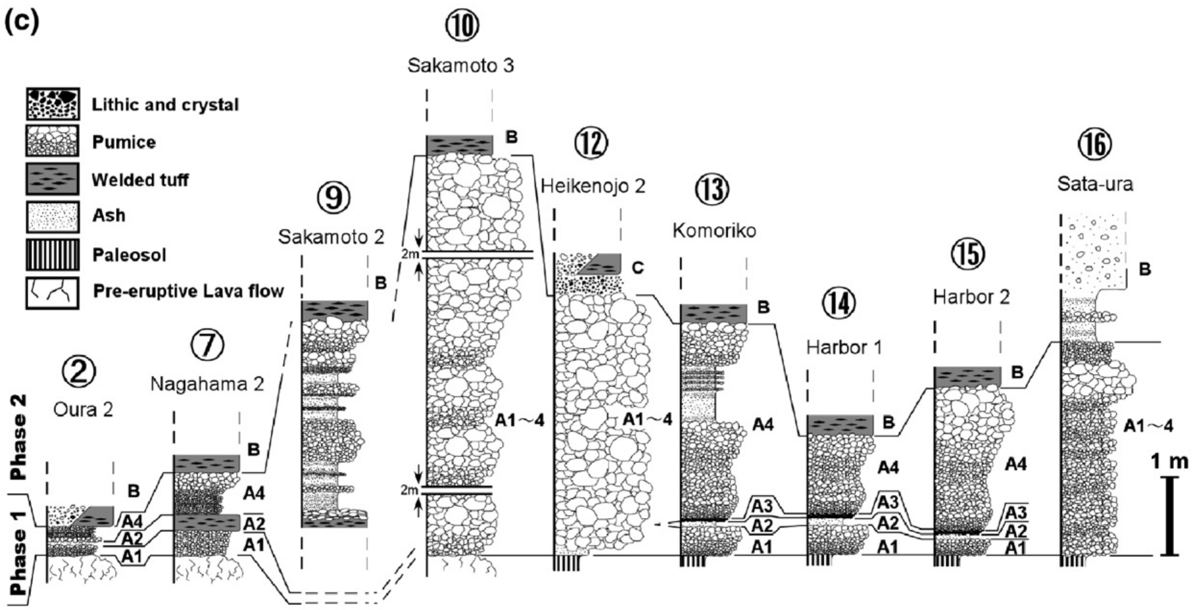

Fig. 3 (*continued*).

(Satsuma Iwo-jima and Take-shima; Fig. 2), display various lithofacies. The pyroclastic density current deposits display massive, stratified, and cross-stratified facies with various degree of welding, that are interpreted as traces of spatial and temporal change of pyroclasts sedimentation. The composite sections of Fig. 3 illustrate the stratigraphic relationship between layers and units of the deposits. On these islands, they are divided into three major units; Unit A, pumice-fall deposits; Unit B, stratified pyroclastic density current deposits with cross-bedding; Unit C3 is an ignimbrite (the Koya–Take-shima ignimbrite) with a maximum thickness of 30 m, which runs out about 100 km in maximum over the East China Sea (Walker et al., 1984); and Unit D is co-ignimbrite ash-fall deposits approximately contemporaneous with the Unit C3 deposition, and is not identified in proximal areas, but well recognized on mainland Kyushu. The pumice fall of Unit A is underlain by subjacent brown paleosol, which developed on the top of the 8–13 ka Komorikô tephra group (Okuno et al., 2000) in Take-shima and on northern side of Satsuma Iwo-jima. However, on the western side of Satsuma Iwo-jima, Unit A is underlain by the Nagahama lava (rhyolite). At some proximal locations, Unit B and the lower part of Unit C (Units C1 and C2) are absent, so that the upper part of Unit C (Unit C3) rests directly on Unit A. This is because of localized non-deposition or erosional removal of lower units by the upper ignimbrite. Each unit or subunit of the 7.3 ka deposits is also composed of several distinctive layers that can be correlated from exposure to exposure throughout the islands. The layers have structures, appearances, and origins that justify their designation as units.

The 7.3 ka deposits are distributed widely along the southern Kyushu mainland, Kuchinoerabu-jima, Tanega-shima, and Yaku-shima (Fig. 1). In these areas, Unit C3 is mainly deposited and Unit A is limited to the eastwards. Unit B is not deposited and is only identified in proximal two islands.

3.1. Unit A (Plinian fallout deposit, Phase 1)

Unit A is characterized by pumice lapilli and ash-rich layers divided into four subunits A1, A2, A3 and A4 (Figs. 3c and 4a). Units A1 and A2 are traceable from the Kikai caldera to southern Osumi Peninsula (Fig. 5a, b). Unit A3 is only deposited in the Satsuma Iwo-jima and Take-shima. In addition, A4 is traceable from the Kikai caldera to the Satsuma and Osumi Peninsulas over the East China Sea (Fig. 5c, d). Here, we refer to some of the geological data of Unit A on mainland Kyushu from Ui (1973) and Walker et al. (1984), because we could not survey Unit A in detail, due to presently decreasing outcrops.

A1 comprises a normal-graded layer of clast-supported white to pinkish pumice lapilli, less than 5 cm in size, and subordinate lithic lapilli, less than 3 cm in size. Lithic lapilli include fresh and hydrothermally altered ones, and crystals of feldspar and pyroxene are

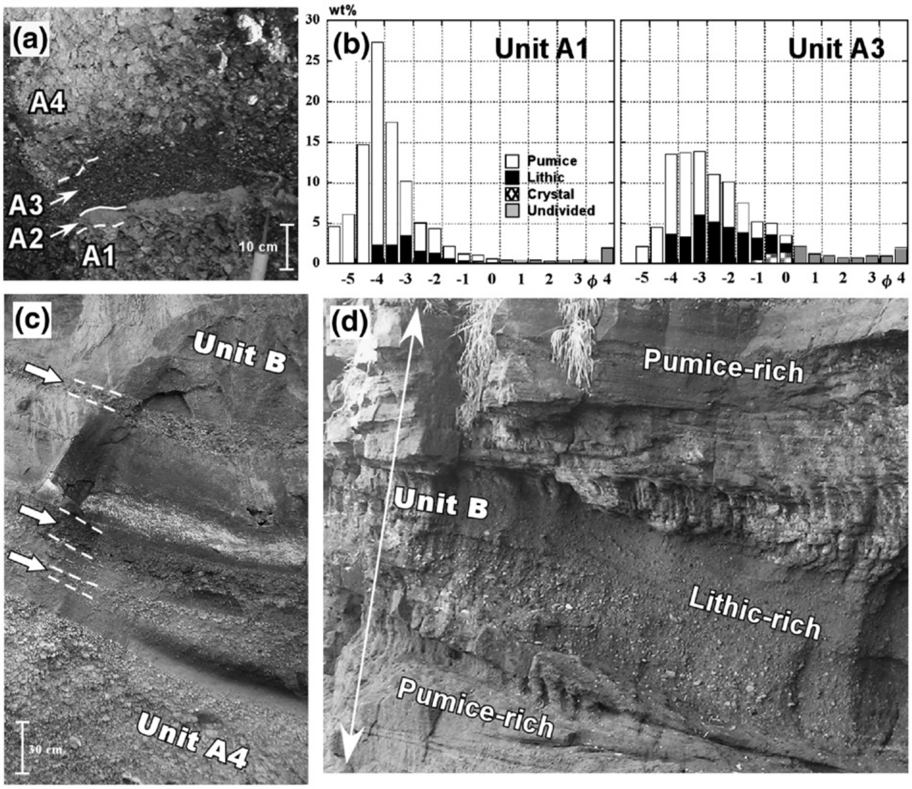

Fig. 4. (a) Unit A pumice fall deposits are subdivided into four subunits (Units A1, A2, A3, and A4) at location 14 (Take-shima harbor). The boundary between Units A2 (ash-fall) and A3 (lapilli-rich fall) is sharp. This indicates a small time gap between Units A2 and A3 deposition. (b) Histograms of granulometry of Units A1 and A3. Unit A1 mainly comprises pumice lapilli, which is covered by fine ash, Unit A2. In Unit A3, lithic and free-crystals increase considerably. (c) Unit A4 plinian pumice fall deposits and Unit B intraplinian flow deposits at location 16 (Sata-ura in Take-shima). Arrows show pumice fall layers embedded by Unit B. Unit B shows weakly welded stratified to non-welded massive facies. (d) Representative lithofacies of Unit B, which is characterized by welded pumice-rich and lithic-rich stratified facies at location 9. Scale arrow is about 3 m.

also included as minor components. A1 thickens to a maximum of 30 cm and occurs mainly on Take-shima (Figs. 3c and 4b).

A2 mainly comprises a layer of white to grayish fine ash, bearing obsidian clasts, less than a few mm in size, which thickens to about 5 cm in Take-shima and at Oura (location 2) in Satsuma Iwo-jima. Near Nagahama (location 7) in Satsuma Iwo-jima, A2 changes to a weakly welded flow deposit, comprising poorly-sorted orange to reddish-colored fine ash and deformed pumice. Although the contact between A1 and A2 is diffuse or gradational, the contact between A2 and A3 is sharp (Fig. 4a). In some cases the lower parts of ash-rich layers contain abundant pumice clasts. On Osumi Peninsula, Units A1 and A2 are only distributed in the southern area (Fig. 5a, b).

A3 is the layer richest in lithic lapilli and crystals of Unit A (Fig. 4b), which consists of hydrothermally altered ones, and crystals of feldspar and pyroxene. The contact between A3 and A4 is gradational, and the content of lithic lapilli and crystals gradually decreases into A4 (Fig. 4a, b).

A4 is the coarsest and thickest layer in Unit A. It is more than 3 m thick near Heikenojo (location 12) on Satsuma Iwo-jima, and has a more extended distribution with a NE dispersal axis from the Kikai Caldera to Osumi Peninsula on the Kyushu mainland, where it is still more than 50 cm thick (Fig. 5c, d). It comprises a normal-graded layer of clast-supported white to pinkish pumice lapilli, less than 50 cm in size, and subordinate lithic lapilli, less than 10 cm in size, near the Kikai caldera. In the upper part of A4, beds of pumice lapilli are interbedded with a few layers of non-or weakly welded pyroclastic density current deposits, Unit B (Figs. 3c and 4c). The boundary between Units A and B cannot be defined clearly. On the steep slope of a topographic depression in the vicinity of Sakamoto in Satsuma Iwo-jima (location 10), A4 is more than 3 m thick with more than ten subunits of reversed-grading pumice lapilli (Fig. 3c). The layers show thickness variations, indicating deposits originating from the remobilization of pumice lapilli at higher levels on the caldera rim during the eruption.

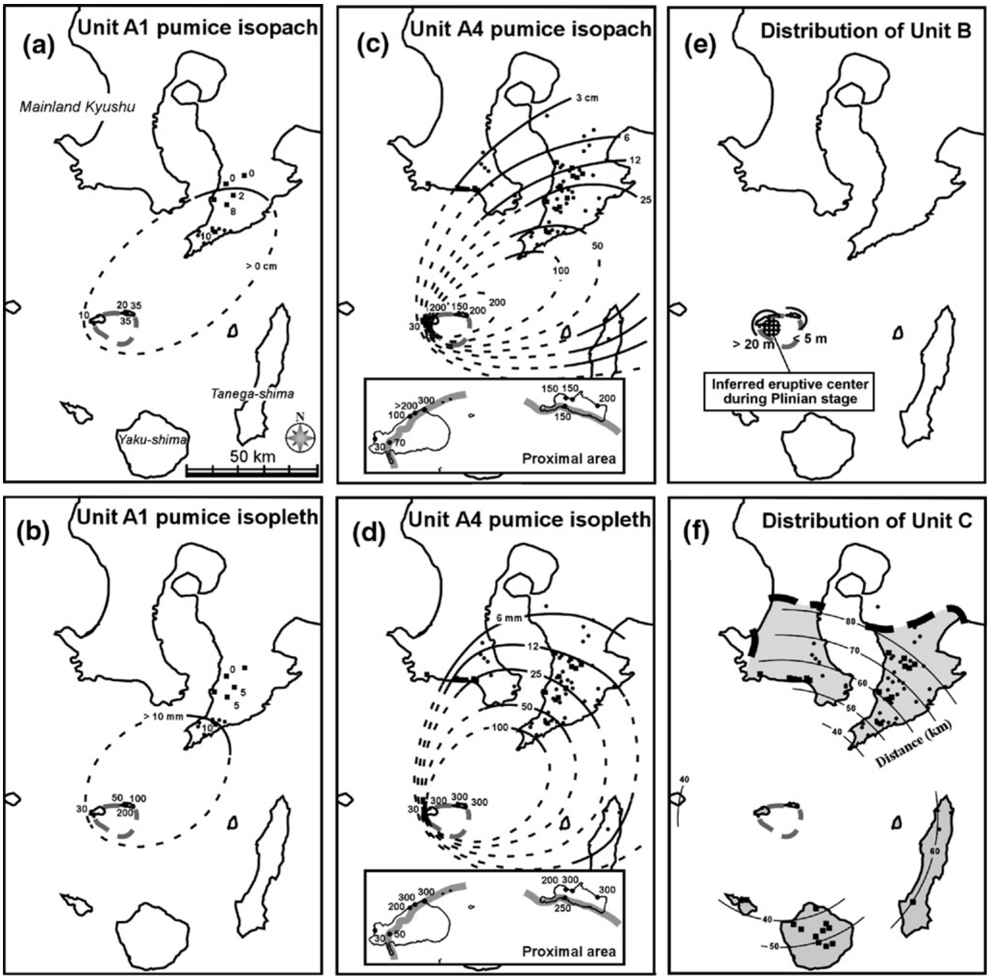

Fig. 5. (a) Isopach and (b) isopleth maps of Unit A1 pumice fall deposit, and (c) isopach and (d) isopleth maps of Unit A4 of the 7.3 ka eruption. Units of isopach and isopleth maps are cm and mm, respectively. (e) The thickness of Unit B and the inferred eruptive center during Phases 1 and 2. (f) Distribution of Unit C. Closed circles in distal area (Kyushu mainland and Tane-ga-shima) in (a) and (b) and shaded area in (f) are based on data from Ui (1973). Closed circles in the distal area in (c), (d), and (f) are data from Walker et al. (1984). Closed circles in the proximal area and closed squares in the distal area are data from this study.

The densities of pumices were measured in the 20–40 mm size range, from the plinian fall (Units A1 and A4) at two locations (locations 13 and 15) in order to determine the eruption column height and the intensity of the plinian phase (see discussion below). The bulk pumice density ranges from 0.24 g/cm^3 to 0.75 g/cm^3 for 41 samples and the average is approximately 0.5 g/cm^3.

3.2. Unit B (intraplinian pyroclastic density current deposits, Phase 2)

Unit B mainly occurs in topographic lows of Satsuma Iwo-jima and Take-shima (Figs. 3, 4c, d and 5). It is much thicker in Satsuma Iwo-jima, mainly depositing in north-western side of the caldera than eastern side, Take-shima.

On the western side of Satsuma Iwo-jima (locations 1, 4, and 7), the stratified deposits are densely welded and sometimes include lithic-rich lenses (a few meters long). On the other hand, on the northern side of the island (location 9), coarser pumice-rich lenses and low-angle cross stratification with minor pinch and swell layers are abundant. Stratified and cross-stratified beds also occur in close proximity with various degree of welding (Fig. 6a). The whole unit can be seen as alternating thin lithic-rich layers or pods and pumice-rich layers. It looks like that a pair of a lithic-rich layer and a pumice-rich layer show one individual aggrading unit by pyroclastic density currents. Although the total thickness varies from a few meters to about 20 m, each thin layer is only from a few to a few tens centimeters thick. At some locations, spheroidal obsidian bombs, which are up to 20 cm in long-axis in size, are included in the lower part of Unit B. The units often indent pumice-fallout units, and are mostly thin towards higher altitudes of the caldera wall. A cooling unit was not identified clearly in the entire Unit B. Its color ranges from black in non- or weakly welded outcrops to dark-reddish in densely welded equivalents.

Unit B is traceable to more distal exposures at Take-shima, but the total thickness is only a few tens of centimeters to a few meters. From locations 13 to 15,

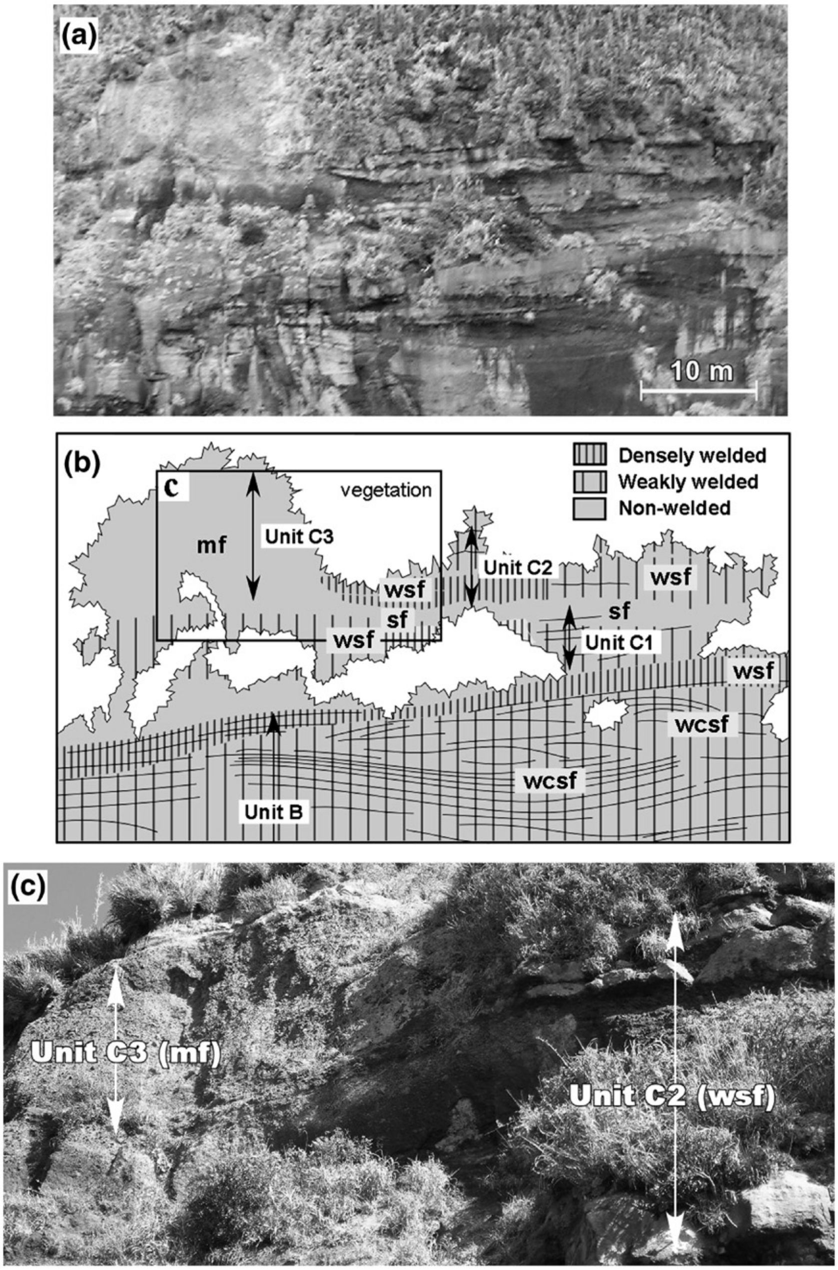

Fig. 6. (a) A photograph and (b) a sketch of Units B and C with various lithofacies and degrees of welding, viewed from sea at location 9 (Sakamoto in Satsuma Iwo-jima). The lower part is Unit B with surge-like cross-stratified or stratified facies. The upper part is Unit C. sf: non-welded stratified facies, wsf: welded stratified facies, wcsf: welded cross-stratified facies, mf: non-welded massive facies. (c) Magnification of Unit C. Unit C1 with non-welded stratified facies and Unit C2 with welded stratified facies gradually changing into non-welded massive facies. (d) A photograph of Unit C with various lithofacies and degrees of welding, viewed at location 1 (Oura in Satsuma Iwo-jima). (e) Unit C3 with non-welded massive facies and (f) Unit C2 with welded stratified facies.

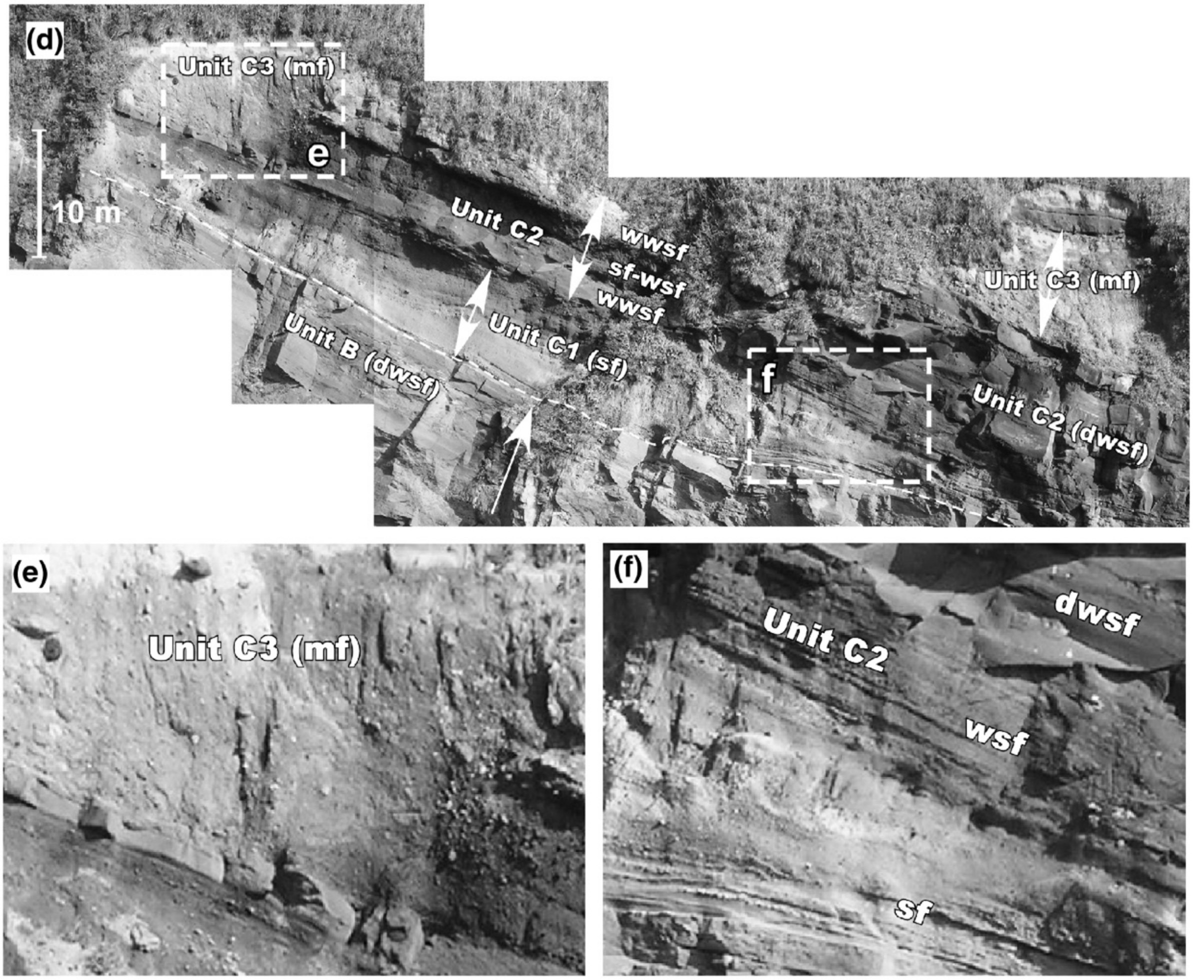

Fig. 6 (*continued*).

Unit B is weakly welded, and completely stratified with embedding some pumice-fall layers (<10 cm in thickness). Lithic-rich layers cannot be recognized. In more distal exposures (location 16), lithofacies show non- or weakly welded and massive.

3.3. Unit C (ignimbrites, Phase 3)

Unit C is divided into three subunits, C1, C2, and C3. Units C1 and C2 are mainly deposited in topographic lows in Satsuma Iwo-jima. In proximal areas, these subunits are gradually connected with each other (Figs. 3, 6, and 7). Unit C3 is found at higher altitudes and distal areas and is traceable from the caldera to neighboring islands and mainland Kyushu (Fig. 5f). It changes its lithofacies with distance from Unit C3a to C3b and C3c.

Unit C1 is fines-poor and lithic-rich, with a total thickness of less than 5 m. The unit is characterized by repetition of inversely to normally-graded layers. In most of the outcrops, transverse sections with stratification through the unit commonly show repetition of strata from millimeters to centimeters thick that gradually splay and become partly diffuse, which is described as diffuse stratification (e.g. Branney and Kokelaar, 2002; Fig. 7a). In the northern part of Satsuma Iwo-jima, inverse-grading from pumice-rich to lithic-rich is recognized in 1.5 m thick in the lowest part of the unit. On topographic highs, the stratified facies of Unit C1 eventually fades out into lithic-rich massive lithofacies when traced laterally across several meters.

Unit C2 is less than 5 m thick and weakly or densely welded stratified. It is composed of lithic-rich layers and densely welded ash-pumice rich layers, similar to the lithofacies of Unit B (Figs. 6 and 7). The thickness of each layer varies from a few tens centimeters to a few meters. Lithic-rich layers include altered lava blocks and

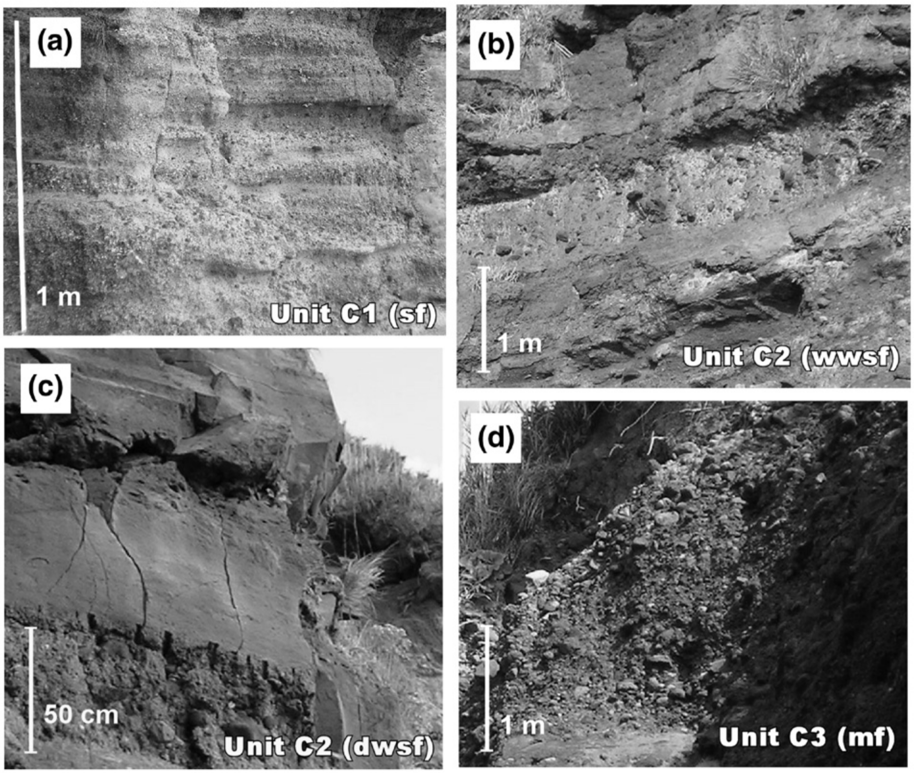

Fig. 7. (a) Non-welded stratified facies (sf) of Unit C1 (location 5). (b) Weakly welded stratified facies (wwsf) of Unit C2 (location 9). (c) Densely welded stratified facies (dwsf) of Unit C2 (location 9). Unit C2 includes boulders some of which make sag-structures. Components of non- or weakly welded units are mainly altered lithics. (d) Non-welded lithic-rich massive facies (mf) of Unit C3a (location 9).

boulders, less than 40 cm in size. Some boulders make sag-structures. Fiamme occur in densely welded parts. The color of the welded tuff units is reddish to grayish. In the most proximal location (location 6), a degree of welding is low and the boundary of Units C1 and C2 is unclear.

Unit C3 has various characters of ignimbrite lithofacies over distance, which is related to the lateral variations of thickness (Fig. 8), internal structure, and the amount of lithic material, and is subdivided into Units C3a, C3b, and C3c, based on differences in its lithofacies.

Unit C3a is characterized by massive, extremely fines-poor and lithic-rich ignimbrite with normal or no grading up to 10 m thick. In the lower part of the unit, stratified beds sometimes occur, which can be recognized only in Satsuma Iwo-jima, especially at high altitudes (locations 6, 8, 9, and 12). At location 8, lithics are less than 2.5 m in size, but pumice is less than a few tens centimeters. At other locations, lithic and pumice are less than 50 cm and a few tens centimeters, respectively. The deposits are reddish or grayish in color, reflecting a large amount of lithic material. The unit continues from the stratified facies of Units C1 and C2 without sharp contacts (Fig. 6). In Satsuma Iwo-jima, although the contact relationship indicating a significant time-break between Units C1 and C3 cannot be observed, some erosional signatures on edges of welded Unit C2 are found.

Units C3b and C3c are characterized by a basal lithic-rich layer and overlying pumice–ash-rich ignimbrite, respectively. These facies occur at locations 1 and 2 (Oura) in Satsuma Iwo-jima, in Take-shima, and distal exposures in neighboring islands. Unit C3b is basically massive, fines-poor, and up to a few meters thick. It includes pumice and lithic less than 50 cm in size. Lithics are composed of boulder-like rounded lava and altered or fresh lava. In distal islands, the unit becomes up to a few centimeters thick and mainly composed of accidental lava and crystals. Unit C3c is massive and pumice–ash-rich, and up to 30 m thick in Take-shima and about 1 m thick in neighboring islands. In Take-shima, the unit may be subdivided more because weak stratifications (boundary-like) and lens-shaped segregation pods can be observed at locations 14 and 16. The unit includes pumice, obsidian clasts, and other lithic

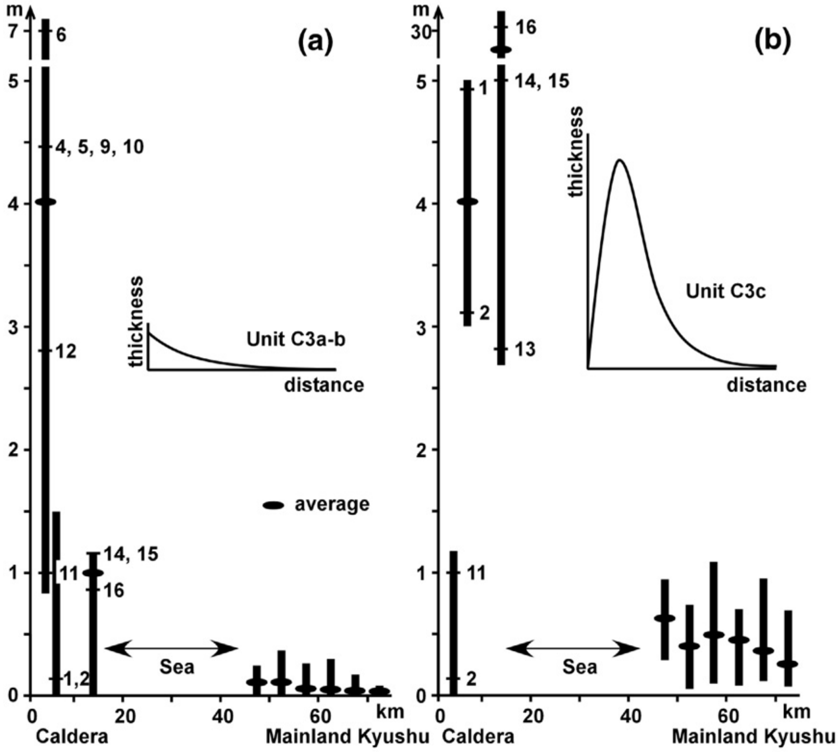

Fig. 8. Range and average values for the thickness of (a) Units C3a–b and (b) Unit C3c on proximal and distal areas. Distal data are combined with ones from Walker et al. (1984), which are averaged for sites in 5 km intervals of distance from the Kikai caldera.

fragments less than a few tens centimeters in size. The deposit is whitish in color, reflecting a large amount of pumice and ash. In distal islands, Unit C3c becomes up to a few meters thick in Kuchinoerabu-jima and Yaku-shima, or less than 1 m in more distal areas (Fig. 8). The facies is basically orange or yellowish in color, but is grayish or whitish in some locations (Kuchinoerabu-jima and Yaku-shima). On the southern coast of Satsuma Peninsula, Unit C3 directly lies on the erosion surface of old deposits without Unit A pumice-fallout layers, despite accounts from isopach area of the fall. The erosion surfaces of deposits are also observed in Tane-ga-shima.

The volumes of Unit C3a-b and Unit C3c were roughly estimated to be about 10 km^3 and 20–35 km^3, respectively (15–25 km^3 in total DRE) (see Appendix).

3.4. Unit D (co-ignimbrite ash-fall deposit, Phase 3)

This unit has an extensive lobe with an axis length of over 1000 km, covering most of the southwest to central Japan and the northwest Pacific Ocean (Machida and Arai, 1978), but not deposited in the proximal caldera rim (Satsuma Iwo-jima and Take-shima). It is orange or yellowish in color, and prominently consists of thin glass shards. In southern Kyushu, especially Osumi Peninsula, there are pumice fragments, armored lapilli, and accretionary lapilli concentrated at the base of Unit D. The total volume of this tephra has been estimated to be about 100 km^3, using an isopach map of this tephra (Machida and Arai, 1978, 2003). The DRE volume 50 km^3 is assumed using a deposit-density 1.25 g/cm^3.

4. Faults and timing of caldera collapse

Clues to the timing of caldera collapse appear in the form of a fault overlain by Unit C3 on the caldera rim. Aerial photographs have shown that the fault is located on the edge of an arc-like depression that continues from Komorikô on Take-shima which tilts toward the inside of the caldera (Fig. 9). Subvertical strata (2 m wide and 3 m high) composed of pre-caldera forming deposits Nagase ignimbrite (K-Ns, 95 ka, Ono et al., 1982), Komorikô tephra groups (K-Km, 8–13 ka, Okuno et al., 2000), and a plinian fallout deposit from the initial stage of the eruption, can be found in a tilted block in the fault zone (Fig. 9c, d).

The fault plane has a dip of 85–90 °E and a strike of N20–30 °W. In the faulted zone, tongues of humic soil, comprising the surface of the Komorikō tephra

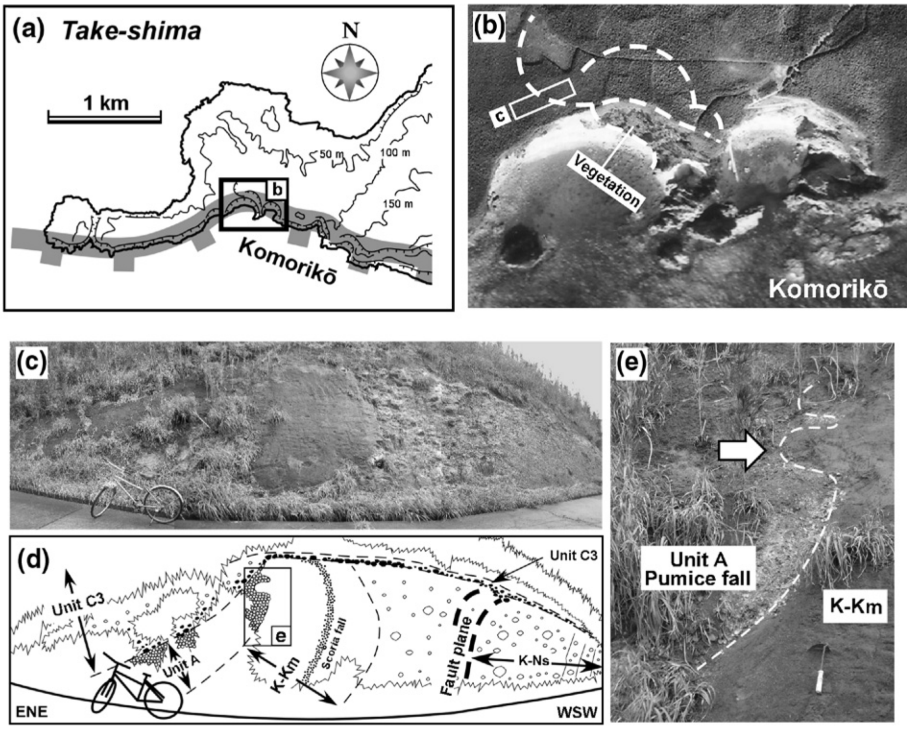

Fig. 9. (a) Location and topography of faults on the south of Take-shima. The shaded area shows the caldera wall. (b) Aerial photograph of the caldera wall near Komorikō. Dashed lines show the rim of the part tilted toward the inside of the caldera. The outcrop of a fault was located on the edge of the arc-like depression continuing from Komorikō. (c) A photograph and (d) a sketch showing the fault cutting through pre-caldera forming deposits (K–Km: 8–13 ka; K–Ns: 95 ka), and with some fissures (right side). The fault shows mainly normal movement, and is directly overlain by basal coarse breccia of Unit C3. Sub-vertical strata composed of pre-caldera forming deposits and plinian fallout are observed in the fault. (e) Tongues of humic soil extending into Unit A pumice fall deposit (arrow) in the fault.

group, extends into the pumice fallout deposits, Unit A (arrow in Fig. 9e). Unit B is lacking in this exposure. A depression on the uppermost surface of the faulted zone is directly overlain by the basal breccia of Unit C, including fragments of the Komorikô tephra group. Normal fault binding blocks of strata that tilt toward the topographic low, indicate that this was an extensional zone during caldera collapse (e.g. Roche et al., 2000). On the other hand, fissures in Unit C on the northern caldera rim of Satsuma Iwo-jima show mainly normal movement or open cracks, indicating that sliding also occurred just after the climactic pyroclastic flow erupted (Kawanabe and Saito, 2002).

Based on these lines of evidence, it is considered that the caldera collapse started before Unit C deposition, or during Unit B deposition. This event may have continued until the end of Unit C deposition.

5. Grain size and components

Grain size and components of Units B and C were analyzed using samples from proximal and some distal areas, and were also compared with data of previous studies (Walker et al., 1984).

In a grain-size plot (Fig. 10; Md$\varphi - \sigma\varphi$ plot and F1–F2 plot), all lithic-rich samples, with two of non-welded lithic-rich layers in Unit B and others of Units C1 and C3, are plotted in the field of fines-depleted ignimbrite (Walker, 1983), which has the same characteristics as the ground layer of ignimbrite in distal areas (Walker et al., 1984). On the other hand, pumice–ash-rich layer (Unit C3c) plots in the field of normal pyroclastic flows, with layer 2 of ignimbrite in distal areas. Grain-size histograms for Unit C (Fig. 11) show that grain size is larger in Unit C3a than Units C1 and C2 in Satsuma Iwo-jima and it decreases in Take-shima, where Units C3b and C3c are dominant rather than Unit C3a, and further decreases in the distal neighboring islands (Fig. 11).

Major components of lithic-rich layers in Unit B are altered lithic, crystals, less vesicular obsidian clasts, pumice lapilli (partially welded), and glass shards. Lithic size is up to 30 cm in long-axis. Components of eruptive materials in Unit C1 were almost the same as

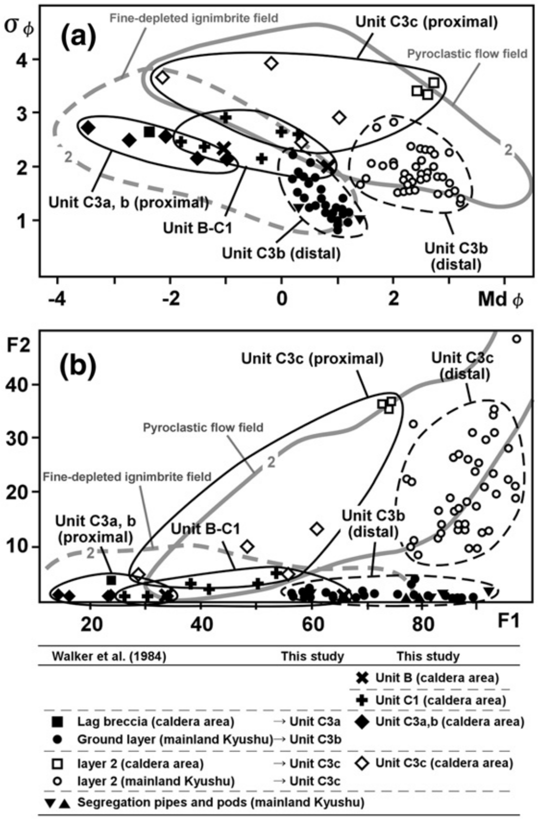

Fig. 10. Grain-size plots of Units C1 and C3 in the 7.3 ka eruptive deposits for the proximal and distal areas. (a) sorting (graphic standard deviation $\sigma\varphi$) vs median diameter Mdφ. (b) F2 (weight percentage finer than 1/16 mm) vs. F1 (weight percentage finer than 1 mm). Gray solid lines: 2% contour for the pyroclastic flow field. Gray dashed lines: 2% contour for the field of fine-depleted ignimbrite facies.

Unit B, and they are subdivided into lithic, crystal, obsidian clasts, and pumice and glass shards (Fig. 12). In some locations (ex. location 10), many boulders are concentrated in the lithic-rich units (Units B and C1). The juvenile clasts range from dense bomb to moderately vesicular pumice. Spheroidal-shaped obsidian bombs with glassy chilled rinds surrounding more vesicular interiors are included in Unit B, and pumice (in proximal) and micro-pumice (in distal) with thin glassy crust and micro-cracks are sometimes included in Unit C (Fig. 13). Their shapes are subspherical, and commonly indicate formation whilst hot and fluidal.

Results of component analyses indicate that lithic and crystal contents change vertically and laterally in Unit C. In the proximal portion, there is a vertical variation with which the lithic-content decreases from Unit C1 to C3a, but the crystal-content increases from Unit C1 to C3a (PCL diagram in Figs. 11 and 13). Unit C3c mainly includes pumice and glass shards with a little amount of lithic and crystals, compared with Units C1 and C3a. Unit C3 has a lateral variation of components such that the unit is richer in lithic than crystals in the proximal area (Unit C3a) but crystals become a major component in the distal area (Unit C3b), (Fig. 11). In distal Satsuma Peninsula, Unit C3b sometimes contains accidental crystals (quartz) and high-silica glass shards, which has resulted from erosion of underlying sediments by the pyroclastic flow body.

6. Chemical composition and temperature of the erupted magma

The whole-rock SiO_2 content of juvenile materials from the 7.3 ka eruption (20 samples of pumice and obsidian clasts) range from 72 to 74 wt.% for Units A, B, and C1–C2, and from 56 to 72 wt.% for Unit C3 (Table 1). The mafic rocks are from the andesitic part of the banded-pumices in Unit C3 at Take-shima. Water concentrations of pre-eruption rhyolite melt were estimated to range from 3 to 4.6 wt.% for the Unit C3 pumice, on the basis of melt inclusion analyses for plagioclase (Saito et al., 2001). The results show that rhyolite magma was gas-saturated (pressure ranges from 80 to 180 MPa) before the eruption (Saito et al., 2001). Although water concentrations of melt inclusions in Units A, B, and C1–C2 were not analyzed, the large variation in water concentration in the Unit C3 melt inclusions was attributed to the result of exsolution of volatile in the magma prior to the eruption. The magma chamber depth was estimated to be 3–7 km from the gas-saturation pressure of these melt inclusions (Saito et al., 2001). In the climactic stage of Unit C3, banded pumices with andesitic composition (SiO_2-range is 56–58 wt.%) came to be included. This indicates that mafic magma co-existed or intruded into a chamber deeper than approximately 7 km. The magma temperature was estimated as about 960 °C by Saito et al. (2003), applying two-pyroxene thermometry to intergrown pyroxene phenocrysts in pumice of climactic stage. This value of temperature is almost the same as that of the present Iwo-dake rhyolite, 950–1000 °C, which was also estimated by Saito et al. (2002) using two-pyroxene thermometry.

7. Dynamics and time-scale of Plinian phase

Phase 1 of the 7.3 ka Kikai eruption was marked by widespread pumice fallout, Units A1–A4, over the sea around the Kikai caldera. The dispersal characteristics of these pumice-fall deposits preserve important information about the dynamics of the eruption column. The

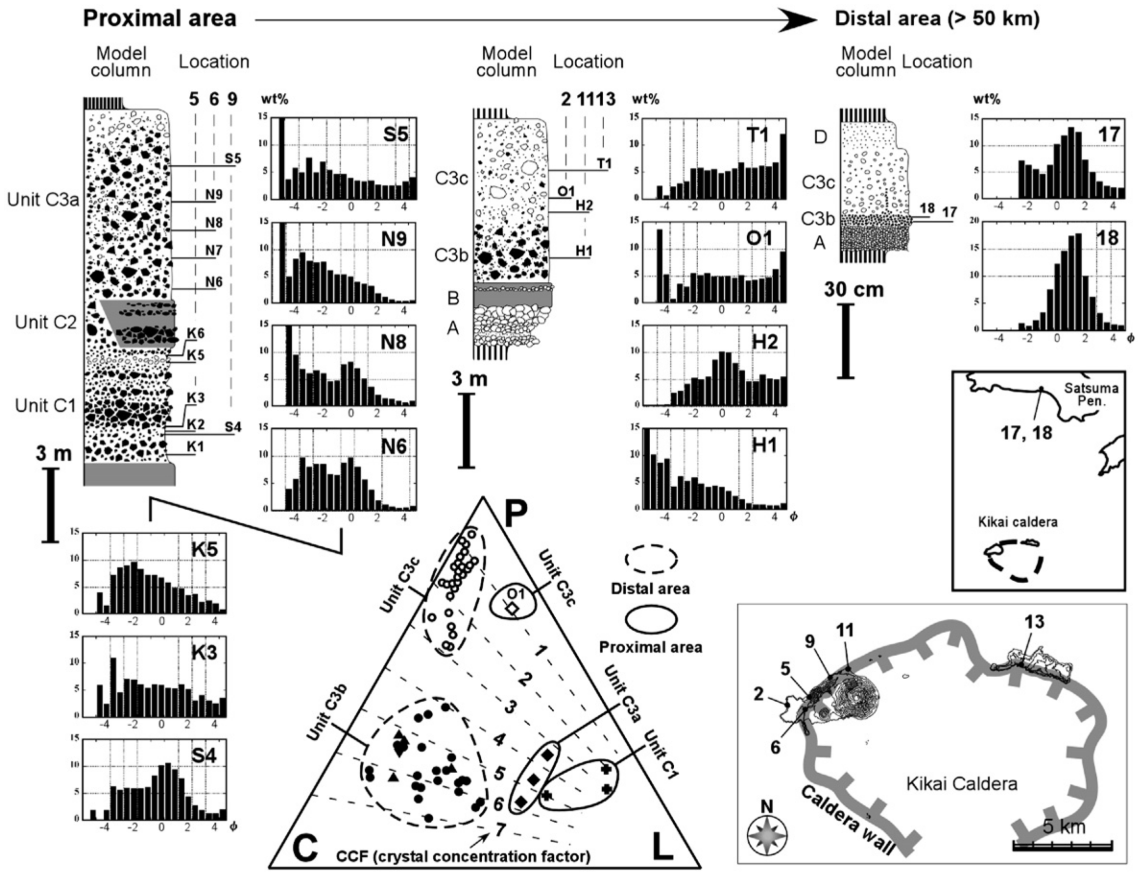

Fig. 11. Sampling localities and sample number for granulometric analyses of the 7.3 ka deposits, and grain-size histograms illustrating the difference in grain size through vertical sections in the proximal area, and the differences in horizontal sections in the proximal (caldera area) and distal (Mainland Kyushu) regions. Lower figure shows weight percentage of pumice + glass shards (P), free crystals (C), and lithic fragments (L) in representative samples of Units B, C1, and C3. Dotted lines show crystal concentration factors. Symbols as Fig. 10.

eruptive vent in Phases 1 and 2 should have been located on the western side of the caldera, probably near the present Iwo-dake volcano, based on the distribution and clast size of the plinian fallout deposits (Figs. 3c, 5a–d, and 14a). The thickness variation of the intraplinian pyroclastic density current deposits (Unit B) also indicates that the source area was located near Satsuma Iwo-jima (Figs. 5e and 14b). Units from A1 to A4 represent two phases of the plinian eruption.

7.1. Column feeding stage

The eruption started with a small plinian column feeding pumice to the south of the Osumi Peninsula (Unit A1; Fig. 5a, b). The plinian eruption was a smaller-scale than in the second phase (Units A3 and A4), based on isopach and isopleth maps. Towards the end of this initial plinian phase, a pyroclastic density current with an ash-cloud was generated by a column collapse near Satsuma Iwo-jima. This event produced flow facies in proximal area and ash-fall facies in distal area (Unit A2). After a short time gap, indicated by a sharp contact between A2 and A3, the main plinian phase started with a vent-widening phase.

In the second phase of the plinian eruption, which produced Units A3 and A4, a large amount of lithics were ejected initially, probably related to the enlargement of the fissure/conduit system. The eruption became more sustained and more vigorous with time. Later, the column was sustained by high discharge rate with minor fluctuations, which is indicated by a few vertical changes of pumice clast size identified at Takeshima. Eruption parameters (column height, tephra volume, and discharge rate) were calculated from field data for the second stage of the plinian eruption. The pumice density data (average approximately 0.5 g/cm^3) was used to adjust the size of the maximum pumice measurements so that the theoretical curves of clast

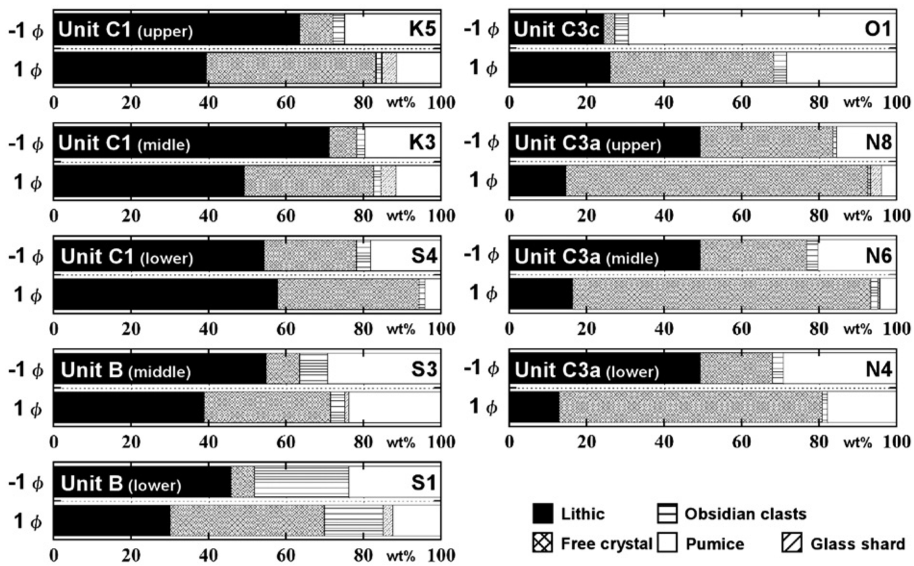

Fig. 12. (a) Component variation through representative vertical sections of non-welded units. Sampling locations (upper right in each diagram) as Fig. 10.

dispersal in Carey and Sparks (1986) could be used to determine eruption column height and intensity of the plinian phase. Lithic lapilli data is lacking in the distal area, because Unit A could not be surveyed in detail due to the current reduction of outcrops. Application of the model also requires knowledge of both the vent

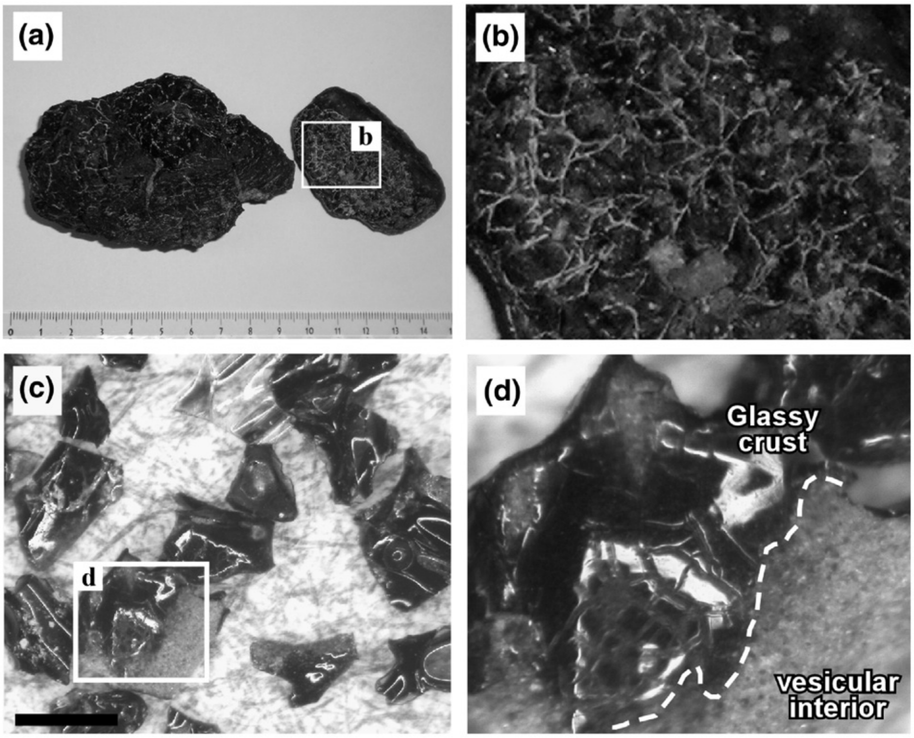

Fig. 13. (a) Spheroidal obsidian clasts, with many micro-cracks developed on their surfaces (b) in Unit C1 at location 9. (c) Pumice fragments covered thin glassy crust with micro-cracks in Unit C3. Scale bar is 1 mm. (d) Magnification of figure c.

Table 1
Whole rock major and trace element compositions of representative samples from 7.3 ka deposits

Whole-rock major element composition									Matrixglass	
No	1	2	3	4	5	6	7	8	1	
	01Ffa1	01Ffa2	04Fpfl1	04Fpfl2	04Fpfl4	00Koapfl	01Tpfl1	01Tpfl2	Kfl	S.D.
Unit	A	A	B	B	C1	C2	C3	C3	B	(n=21)
SiO_2	71.45	71.80	71.81	71.77	71.87	71.38	71.69	58.80	74.89	0.25
TiO_2	0.72	0.71	0.72	0.71	0.72	0.69	0.73	0.92	0.67	0.06
Al_2O_3	13.71	13.63	13.83	13.72	13.75	13.54	13.70	16.23	12.87	0.17
Fe_2O_3 [a]	3.85	3.66	3.72	3.75	3.69	4.11	3.74	8.95	–	–
FeO	–	–	–				–	–	2.62	0.21
MnO	0.10	0.10	0.10	0.10	0.10	0.10	0.10	0.14	0.07	0.05
MgO	0.77	0.73	0.77	0.72	0.72	0.77	0.72	2.75	0.39	0.04
CaO	2.72	2.66	2.35	2.53	2.50	2.67	2.58	7.28	2.08	0.08
Na_2O	3.96	3.96	3.85	3.91	3.79	4.05	3.94	3.29	3.17	0.22
K_2O	2.57	2.62	2.73	2.67	2.74	2.57	2.65	1.40	3.23	0.36
P_2O_5	0.15	0.14	0.13	0.11	0.13	0.14	0.14	0.24	–	–
K_2O+Na_2O	6.53	6.58	6.58	6.59	6.53	6.61	6.59	4.69	6.40	
V	40.1	37.2	n.a.	n.a.	n.a.	44.0	40.0	212.1		
Cr	n.d.	n.d.	n.a.	n.a.	n.a.	n.d.	n.d.	13.9		
Ni	n.d.	n.d.	n.a.	n.a.	n.a.	n.d.	n.d.	0.3		
Rb	71.7	73.4	n.a.	n.a.	n.a.	72.4	73.5	37.2		
Sr	161.4	158.9	n.a.	n.a.	n.a.	162.0	156.6	251.7		
Ba	339.6	359.2	n.a.	n.a.	n.a.	352.1	344.8	217.2		
Y	35.6	34.1	n.a.	n.a.	n.a.	35.2	34.3	24.7		
Zr	186.2	187.1	n.a.	n.a.	n.a.	190.4	191.7	111.4		
Nb	5.5	5.7	n.a.	n.a.	n.a.	4.9	6.0	3.4		

Unit: wt.%.
All iron calculated in FeO for groundmass glass composition.
S.D. = standard deviation of electron probe micro-analyses.
Analytical procedures: Major element compositions were determined by X-ray fluorescence analysis (XRF) as described in Yajima et al. (2001). Groundmass glasses were analyzed by electron microprobe (JEOL JSM-5410 with wavelength dispersive solid state detector of Oxford Link ISIS) using defocused electron beam of 10–20 µm in diameter, accelerating voltage of 15 keV, and selecting random points (number of parentheses; n) in each thin section.
[a] Fe_2O_3 is total Fe as Fe_2O_3 for whole-rock major element composition.

location and the half width of clast isopleths perpendicular to the main dispersal axis. In the case of Units A3 and A4, the limited number of proximal exposures makes it difficult to define the main dispersal axis precisely. However, examination of the exposures relative to the vent and clast size variations between outcrops shows that the minimum possible half widths are obtained by assuming the dispersal axis is in the NE–SW direction (Fig. 5c). As a result, the column height is estimated to be 40–43 km, and the wind velocity is calculated to be 40 m/s. The total tephra volume of the plinian stage was also estimated from a relationship between isopach area and thickness of fall units, using Pyle's (1989) method, to be about 40 km^3. This volume of about 40 km^3 corresponds to a DRE magma mass of 2×10^{13} kg. Using values of magma mass and column height, the discharge rate during the plinian eruption was estimated to be 2×10^8 kg/s from a thermofluid dynamical model (Woods, 1988), assuming an initial magma temperature of 1200 K, which is estimated from petrological data. Moreover, the eruption duration estimated from magma mass data and discharge rate was at least 28 h. Units A3 and A4 represent a single eruptive unit that records a single explosive eruption. Therefore, the plinian eruption was sustained over a period of one day. A maximum total thickness of 200 cm of fall deposit of the proximal area yields an average accumulation rate of 0.037 mm/s, which is in good agreement with values found for other historic plinian eruption with similar peak intensity, such as S. Maria 1902, Tarawera 1886, Tambora F4, Vesuvius 79, and Pinatubo 1991 (Carey and Sigurdsson, 1989; Scott et al., 1996; Rosi et al., 2001).

7.2. Column collapse stage

Unit B consists of intraplinian pyroclastic density current deposits, which may have been derived from

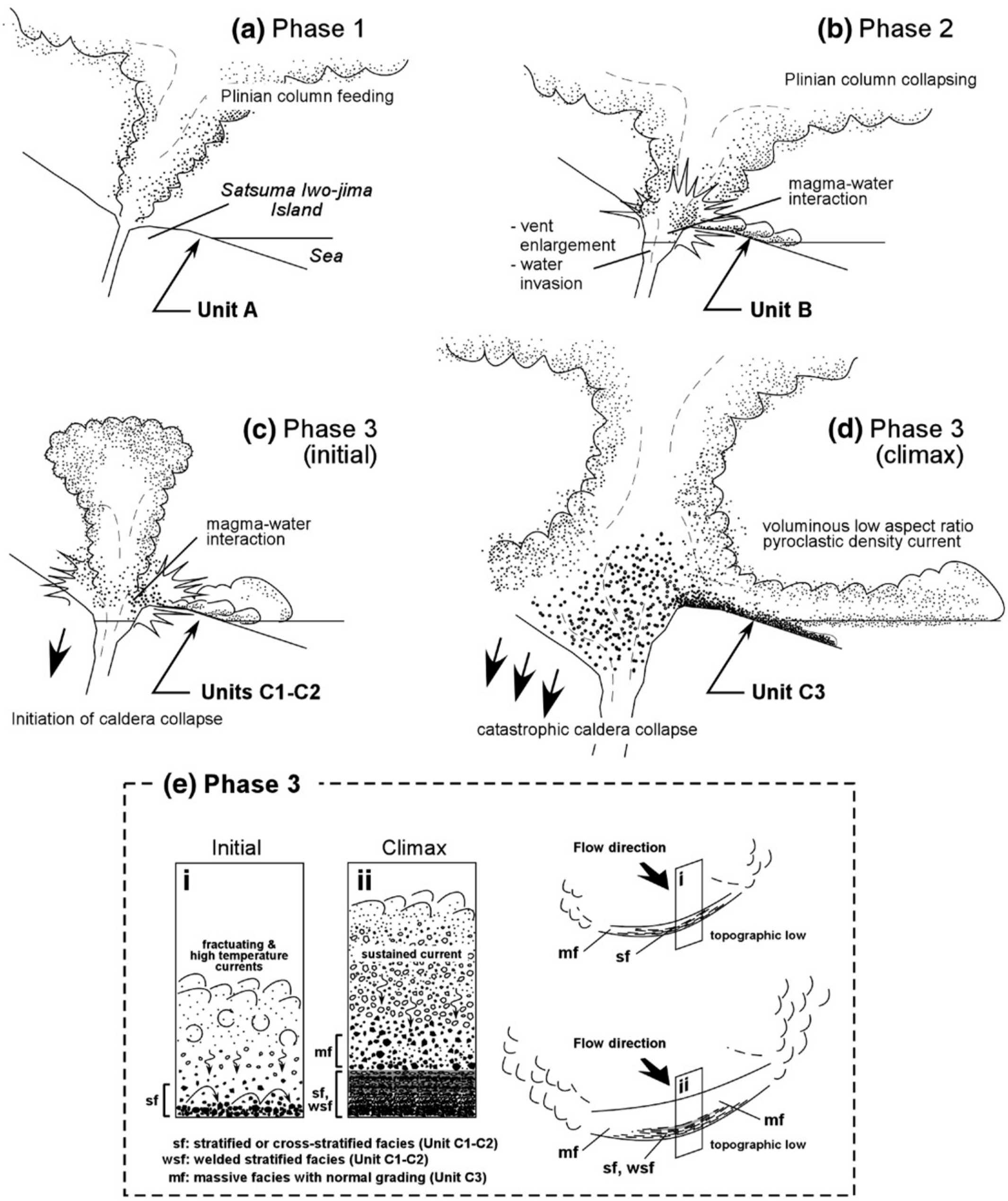

Fig. 14. Idealized processes during a 7.3 ka marine caldera-forming eruption at Kikai volcano. (a) Plinian eruption occurred near the Satsuma Iwo-jima (Phase 1). (b) Plinian column collapsing with magma–water interaction and pyroclastic density currents were generated from the base of the column (Phase 2). (c) Initial of caldera-forming stage. Magma–water interactions occurred during vent-widening. (d) Climax of caldera-forming stage, which is accompanied with catastrophic caldera collapse and generation of a low-aspect ratio pyroclastic density current traveling over the sea. (e) Cross sectional models of climactic voluminous pyroclastic density currents. (i) Initial phase is characterized by fluctuating and high temperature pyroclastic density currents, resulting in stratified Units C1 (non-welded) and C2 (welded). Unit C1 is derived from segregated dense materials (lithic and free-crystal) and Unit C2 is mainly from elutriated ash and pumice-rich flows. These flows occurred in topographic lows and buried them. (ii) Climactic phase is characterized by a sustained current, resulting in non-welded massive facies. In this phase, andesitic banded-pumice became included.

collapse of the plinian column and attributed to changing conditions during the course of the eruption. Conditions which favor the collapse of an eruption column generally include a decrease of water contents in magma or enlargement of eruptive vents (Sparks and Wilson, 1976; Wilson et al., 1980), or magma–water interaction (Koyaguchi and Woods, 1996). Combinations between these conditions are also likely.

The column collapse during the Phase 2 may have been mainly caused by a breakup of conduit under water, because accidental altered lithics are abundant but quenched juvenile materials and boulders are rare in the lithic-rich layers or pods. The accidental lithics may have been derived from the breakup of the walls of the conduit wall abrasion due to fluid flow (Macedonio et al., 1994), as well as from wall collapse due to the pressure change in the conduit during magma ascending (Papale and Dobran, 1993) or magma–water interactions (Dobran and Papale, 1993).

Sedimentary characteristics of Unit B are similar to pyroclastic surge deposits, indicating that dense pyroclasts were well segregated, resulted in lithic-rich layers or pods. Pumice-rich lenses and low-angle cross stratification with minor pinch and swell layers are also typical of deposition from relatively low concentration, traction-dominated turbulent pyroclastic density currents (e.g. Sohn and Chough, 1989).

On the basis of lithofacies and grain analyses, on the northern side of Satsuma Iwo-jima, lithic-rich layers and pumice-rich layers, or a pair of these layers, represent probably one individual aggrading unit. It is proposed that lithics segregated within a current body where elutriated fine and lighter materials were progressively deposited on top and more distally, and this process occurred repetitively during the column collapse phases. Although pulsing or multiple flows were continuously generated and deposited in Satsuma Iwo-jima, only some large-scale currents arrived in more distal regions (Take-shima).

8. Evolution of climactic pyroclastic flows

Units C corresponds with the most devastating phase of the 7.3 ka eruption. Lateral and vertical variations of lithofacies and grain characteristics from Unit C1 to C3 show that Unit C was derived from the climactic eruptive phase but was produced by spatially and temporally evolving sedimentation processes of pyroclastic density currents. Although there are no contact relationship indicating a significant time-break between Units C1 and C2 in Satsuma Iwo-jima, erosional signatures on welded tuff of Unit C2 are partially recognized in the deposit, which may show a short-time gap between Unit C2 and C3. Proximal coarse deposits in Units C1–C3 are interpreted as lag breccias, which are probably related to caldera formation (Walker, 1985; Druitt and Bacon, 1986). Units C1 and C2 only occur in Satsuma Iwo-jima and the sizes of lithics in the proximal breccia are largest near the north of Satsuma Iwo-jima. This area is very near the inferred vent of the plinian phase. Therefore, it is suggested that the source in the climactic phase had a bias toward the western side of the caldera, rather than complete ring-fissure vents.

8.1. Emplacement process

Unit C1 is characterized by repetition of inverse-to normal-grading, fines-depleted, lithic-rich layers, especially in topographic lows, and the stratified facies eventually fades out into massive lithofacies when traced laterally into topographic highs. The stratified facies with lithic-rich graded beds (Fig. 7a) is interpreted to have been produced by dense pyroclasts settled from a current body with fluctuations of shear rates or deposition rates (e.g. Branney and Kokelaar, 2002). The massive facies is interpreted to be the result of high particle concentration in basal part of a moving sustained current. On the basis of these considerations, it is suggested that a pyroclastic density current in the initial of climactic phase had two flow conditions in the body and the two conditions were gradual, reflecting the underlying topography (Fig. 14c, e).

During Unit C2 deposition, higher mass fluxes of currents limited the bulk dilution of the erupting mixture by entrainment of air resulting in higher initial temperatures (Freundt and Bursik, 1998). The heat of juvenile pyroclasts was dissipated slowly provided by the rapid accumulation of pyroclasts in the near-vent area. In the currents, pyroclasts could have been well segregated, resulting in weakly or densely welded stratified deposits, including pumice–ash-rich layers and lithic-rich layers. In addition, boulders and quenched fragments in Units C1 and C2 show that the erupted magma in the initial of climactic phase was interacted with sea water (Fig. 14).

In the climax, a dramatic increase in the mass-flux of a pyroclastic density current is apparent, with the generation of the sustained flow body from which Unit C3 was deposited (Fig. 14). In the proximal area, the current deposited Unit C3a in the near-vent area, and segregated gravitationally along its length depositing Unit C3b, while the more buoyant upper parts resulted in Unit C3c. C3c is interpreted as having been deposited from the relatively dilute and stratified flow consisting of dense lithic-rich lower layers and expanded pumice-rich upper layers into a turbulent low-concentration giant flow with distance. The lower lithic-rich layer in distal area is fines-depleted often accompanied with voluminous ignimbrite (e.g. Walker et al., 1981; Freundt and Schmincke, 1985; Druitt and Bacon, 1986). In the slightly distal regions (Take-shima), the body of pyroclastic density current may have been cooled, and resulted in the non-welded ash-pumice rich ignimbrite (Unit C3c) with a thin basal breccia layer (Unit C3b). This characteristic may be related to dual behavior of the pyroclastic flows, with ash-pumice rich flows traveling over sea to deposit Unit C3c and a lithic-rich Unit C3a or C3b entering sea, as suggested for sea surface and underwater flows from historical eruptions of Krakatau (Sigurdsson et al., 1991) and Mont Pelée (LaCroix, 1904). Thus, eruptive and transport processes of materials caused widespread deposition of low-aspect ratio ignimbrite

On the southern coast of Satsuma Peninsula Unit C3 directly lies on the erosion surface without pumice fallout layers, which is a typical lithofacies of this area, as indicated by Maeno et al. (2006). In near-vent area, the erosion surfaces exist on underlying welded tuff. The lack of pumice fall deposits (Unit A) and the erosion surfaces indicate substrate shearing caused by just-deposited voluminous ignimbrite, as observed at the base of deposits of the blast-initiated pyroclastic density currents of Mount St Helens (Fisher, 1990) and Bezymianny (Belousov, 1996).

Elutriated ash was transported to the more distal areas, and deposited as co-ignimbrite ash-fall, Unit D, includes accretionary lapilli in mainland Kyushu. The climactic pyroclastic flow also includes andesitic banded-pumices, probably derived from the deeper part of the magma chamber.

8.2. Generation mechanism

Low-aspect ratio pyroclastic flows are though to result from high magma discharge rate and the high momentum imparted to the pyroclastic flow when catastrophic collapse of a high eruptive column occurs (Taupo, Walker et al., 1980; Tosu, Suzuki-Kamata and Kamata, 1990; Campanian, Fisher et al., 1993; Rattlesnake, Streck and Grunder, 1995; Kidnappers, Wilson et al., 1995). In the 7.3 ka Kikai eruption, there is no evidence for a high column immediately preceding the climactic pyroclastic flow phase, but it is suggested that the eruption from a single or small vents system may have resulted in high ejection velocities and the production on low-aspect ratio ignimbrite. Legros et al. (2000) suggest that the discharge rate is an order of magnitude smaller in ring-fissure conduits than in single cylindrical conduits, due to the higher friction, based on numerical simulations. Their results also indicate that widespread ignimbrites, which record high-discharge rate eruptions, are not necessarily the result of ring fissure opening during caldera collapse. For the 7.3 ka Kikai eruption, the source of climactic pyroclastic flow had a bias toward the western side of the caldera, thus, the single or small vents system is more favorable than complete ring-fissure system, although the exact vent location has been difficult to pinpoint due to a small number of subaerial outcrops in proximal area.

Magma–water interaction is also a possible scenario, which may have promoted flow mobility because sea water rapidly injected into the vent system can contribute to the expansion and deflation of generated pyroclastic density current (e.g. Wohletz, 1998). The interaction could have imparted a high momentum to the pyroclastic flows, resulting in a radially spreading giant turbulent current. In addition, a coupling of high initial flow velocities, favorable flow paths and emplacement of flows over the sea, for more than 50 km, may have resulted in high turbulence and aided their mobility (e.g. Fisher et al., 1993; Carey et al., 1996).

These two scenarios require more detailed theoretical investigations in future researches, especially about the role of seawater and its effects on the behavior of a pyroclastic flow.

9. Reconstruction of the 7.3 ka eruption

The 7.3 ka caldera-forming eruption is reconstructed from the point of view of its spatiotemporal evolution of pyroclast-transport processes. A time–distance plot showing eruptive sequences and lithofacies variations of pyroclastic density currents is shown in Fig. 15. Phase 1 is characterized by two plinian eruptions where the vent was located near the northwestern side of the caldera. The actual eruption duration of this phase was estimated to be more than one day from the DRE magma mass (2×10^{13} kg) and discharge rate (2×10^{8} kg/s). Phase 1 was followed by column collapse stage of Phase 2. In this phase, high temperature dilute currents were generated during breaks up of the conduit on marine condition. The lithofacies of the deposits are variable from welded stratified or cross-stratified facies in proximal regions, to non-welded massive facies in distal regions. These characteristics probably reflect the sedimentation processes of the high temperature and dilute density currents. Phase 2 gradually became small-scale.

It is suggested that the caldera collapse started before Unit C3 deposition, and that this event continued until the end of Unit C3 deposition, based on fault distribution (this study and Kawanabe and Saito, 2002) and clastic dykes (Naruo and Kobayashi, 2002) (Fig. 15). Naruo and Kobayashi (2002) discussed the timing of the ejection of two clastic dykes related to two large earthquakes found in archaeological sites in southern Kyushu, based on

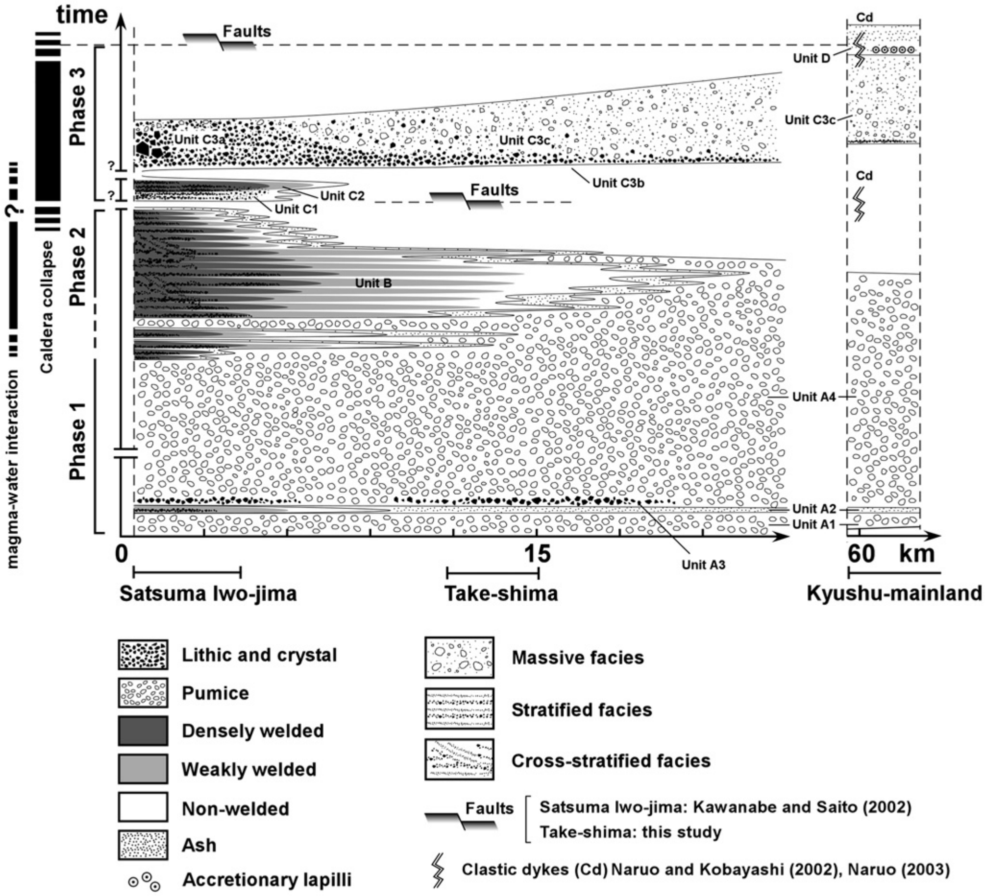

Fig. 15. A time–distance plot showing eruptive sequences and lithofacies variations of pyroclastic density currents during the 7.3 ka Kikai eruption.

precise correlation with tephra and liquefied material. Soft-state deformation of underlying sediment and ignimbrites may relate to seismic shock during the caldera collapse, as reported for other caldera-forming eruptions (e.g. Poris Formation, Brown and Branney, 2004). The first earthquake occurred before the ignimbrite eruption and was much more severe, affecting a wide area of the southern Kyushu mainland and some neighboring islands. On the other hand, the second is thought to have occurred a bit further north during co-ignimbrite ash deposition, affecting only the southern mainland Kyushu (Naruo and Kobayashi, 2002).

Marked influxes of vent-derived lithic clasts (Units C1 and C3a) were followed by deposition from several other caldera-forming eruptions (e.g. Crater Lake, Suzuki-Kamata et al., 1993; Minoan eruption, Santorini, Heiken and McCoy, 1984; Taupo ignimbrite, Wilson and Walker, 1985; Ito ignimbrite, Aramaki, 1984; Kos Plateau Tuff, Allen and Cas, 1998), and can be linked with the onset of the caldera collapse (Druitt and Sparks, 1984; Marti et al., 2000). When enough material was erupted from a magma chamber during the plinian phase, the chamber roof can be no longer supported and a volcanic edifice collapsed to form a caldera (Fig. 14d). With the foundering of the chamber roof into the magma chamber, the pressure of the chamber drastically increased, and the whole highly energetic pyroclastic density current erupted from the western side of the caldera, resulting in the climactic ignimbrite (Unit C3).

To initiate a caldera collapse, erupted mass fractions of plinian eruption need to exceed predicted failure thresholds related to the roof aspect ratio ($R = H$ (roof thickness)$/D$ (chamber diameter)) of the magma chamber (Bower and Woods, 1997; Marti et al., 2000). The failure threshold can be calculated from a theoretical model (Roche and Druitt, 2001) and petrological data (Saito et al., 2001, 2003). The magma chamber depth in the climactic phase can be estimated to be 3–7 km, based on gas-saturation pressure (range from 80 to 180 MPa) of the melt inclusions in plagioclase (Saito et al., 2001). Assuming the cylindrical shape of the magma chamber with 4 km vertical extent, the diameter (D) of it is estimated to be 5 km, using the total volume of erupted magma (70–80 km^3). Moreover, based on this shape and the depth (about 3 km) of the chamber roof (H), the roof aspect ratio is calculated to be about 0.6. On the other hand, the chamber volume fraction erupted before the onset of caldera collapse is estimated to be about 0.1 (=8 km^3 (in the plinian phase)/70–80 km^3 (in the entire eruption)). These eruption parameters (the roof aspect ratio 0.6 and the chamber volume fraction 0.1) can lead to the approximate conditions when coherent (piston) caldera collapse can occur in a theoretical model, using a failure criterion of Roche and Druitt (2001).

10. Effects of seawater on eruption dynamics

Lithofacies and componentry characteristics of the ignimbrites from the 7.3 ka eruption suggest that seawater may have affected eruptive conditions and sedimentation processes to different degrees during the course of the eruption. In particular, we suggest that the degree of mixing of external water and magma during high eruption rates, such as a plinian style eruption, and physical properties of erupted silicic magma played important roles in producing lithofacies variation (e.g. Wohletz, 1998).

The ignimbrites of Phase 2 are characterized by tractionally stratified lithofacies that are densely or weakly welded (Figs. 14b and 15) and consist of alternating layers or pods of lithic-rich and pumice rich layers, with each pair of lithic and pumice-rich layers forming individual flow units. We suggest that during Phase 2 the plinian column collapsed due to the break up of a marine conduit allowing water access to the erupting magma. However, during this stage the interaction between high temperature magma and seawater was limited. Any entrained seawater probably vaporized, promoting a dilution of currents and a segregation of dense lithics including quenched materials. The pyroclastic density currents could be dilute while maintaining high temperature, even in Take-shima 10–15 km from the source and deposit at high temperatures as welding deformation onset.

During Phase 3, there are further interactions between magma and water. Presence of poorly vesicular obsidian clasts, bombs with chilled cracks, and boulders in Units C indicate that erupted magma interacted with seawater and mixed with marine sediments during theinitial climactic phase. The main climactic ignimbrite C3 is largely dry suggesting that the shallow subaqueous plume breached the water surface and was largely subaerial probably resulting from a drastic increase of magma chamber pressure that produced higher ejection velocities and high momentum of ascending magma (e.g. Allen and Stewart, 2003).

The change from wet to dry eruption styles during the 7.3 ka eruption is interpreted to be the result of increasing eruption intensity and/or lower rates of available water, and the sedimentary characteristics of the 7.3 ka ignimbrites are similar to the ones generated from subaerial vents, as observed also in the Minoan eruption, Santorini (Heiken and McCoy, 1984) and 22 ka Aira eruption, Japan (Aramaki, 1984). However, the limited interaction between high temperature magma and seawater in the initial phase appears to have caused the remarkable lithofacies variation of eruptive deposits in proximal near-vent areas, which are characterized by various degrees of welding. We note that in contrast to the Kikai, the Oruanui, Wairakei, and Kos eruptions are characterized by magma–water interactions that continued throughout the eruption and most deposits are fine-grained and rich in accretionary lapilli, while completely lacking a welding profile (e.g. Self, 1983; Allen and Cas, 1998; Wilson, 2001).

11. Implications for a large silicic magmatic system of Kikai volcano

The 7.3 ka eruption of Kikai volcano is the largest (VEI 7) Holocene eruption in Japan. The eruption represents the evacuation of major silicic magmatic system with estimated magma volume of 70–80 km^3 (DRE). The magma chamber depth of the 7.3 ka eruption is estimated to be 3–7 km from the gas-saturation pressure of melt inclusions (Saito et al., 2001). In Unit C3 from the climactic stage, banded pumices with andesitic composition appear indicating that mafic magma co-existed or was intruded into a chamber deeper than approximately 7 km during the 7.3 ka eruption. Postcollapse activity (from 5.2 ka; Okuno et al., 2000) started with the growth of the old Iwo-dake volcano (rhyolitic) on the northwestern side along the marginal faults of the caldera (Fig. 2). The old Iwo-dake magma may be residual of the 7.3 ka magma because the magmas are compositionally similar (Maeno and Taniguchi, 2005) and erupted from almost same location. The basaltic Inamura-dake volcano (from 3.6 ka; Okuno et al., 2000) and the rhyolitic Showa Iwo-jima eruptions in 1934–1935 also occurred in trending with the northwestern marginal faults of the caldera (Fig. 2). The distributions of the 7.3 ka eruptive deposits and postcollapse volcanic edifices indicate that magma sources for both rhyolite and basalt have co-existed in the northwestern side during past seven thousands of years at least. It is also noticeable that the distributions of the vents are just consistent with the southern extension of the western edge of Kagoshima graben (Fig. 1). These lines of evidence indicate that the Kikai caldera is still very active and tends to bimodal activity in the northwestern side, probably associated with the structural weakness of the caldera margin, or extensional faults in the south-western edge of the Kagoshima graben.

12. Conclusions

Sedimentary facies, stratigraphy, and componentry of the pyroclastic deposits of the 7.3 ka caldera-forming eruption at Kikai volcano were investigated mainly in near-vent area and suggest a complex evolution of the eruption from this marine caldera. Stratigraphic sections are characterized by plinian pumice-fall deposits (Units A1–A4), intraplinian pyroclastic density current deposits (Unit B), climactic pyroclastic density currents (Units C1–C2 and C3), and co-ignimbrite ash-fall deposit (Unit D). The eruption duration of the plinian phase was estimated to be a minimum of approximately 28 h, based on clast dispersal data. Collapse of the column produced Unit B, which is characterized by stratified or cross-stratified facies that display various degrees of welding. The sedimentary characteristics indicate that high temperature turbulent density currents were generated in this phase as limited interaction between magma and water was allowed by a breach of the subaqueous conduit system. The climactic phase produced Units C, which is subdivided into three flow subunits (C1–C3). Magma–water interaction is more obvious in the early stages. Unit C1 is mainly non-welded stratified beds, which consist of lithic and crystals, including a minor proportion of quenched juvenile materials. The unit gradually changes into Unit C2, which is a welded stratified beds and consist of lithic-rich layers and pumice-rich layers. Largely climactic eruptions produced Unit C3, a thick and poorly-sorted non-welded massive product, which includes fragments of welded tuff from underlying units in the near-vent area. Sedimentological data suggests that multiple pyroclastic density currents produced Units C1 and C2 in the near-vent area, and were followed by the main sustained current producing Unit C3, a low-aspect ratio ignimbrite, in wide area of southern Kyushu over the sea. The change from wet to dry eruption styles during the 7.3 ka eruption is interpreted to be the result of increasing eruption intensity and/or lower rates of available water. In addition, collapse of the caldera may have started before Unit C3 deposition, and the source had a bias toward the western side of the caldera, rather than ring-fissure vents, through the whole of eruption. The physical volcanology of this study combined with previous work on the petrology and geochemistry reveals the evacuation of a major silicic magmatic system at about 7 km depth that coexisted with or was recharged by mafic magma. The Holocene history of the Kikai volcano records a long term association of mafic and silicic magma.

Acknowledgements

We are grateful to T. Kobayashi, K. Kano, K. Suzuki-Kamata, N. Geshi, and T. Yoshida for discussions and constructive comments and thanks to A. Goto and T. Miyamoto for critical discussions. We are also grateful to Mishima village, Kagoshima, Japan, for the help with our field survey. Reviews by C. Busby, S. de Silva, and an anonymous referee were very helpful in focusing and expressing our ideas. This research was partially supported by the 21st century COE program, 'Advanced Science and Technology Center for the Dynamic Earth' in Tohoku University.

Appendix A

The volumes of Unit C3a-b and Unit C3c can be roughly estimated using the range and average values for the thickness of the deposits (Figs. 8 and A1). The deposit thickness looks like exponentially decaying with distance from the maximum thickness (at Satsuma Iwo-jima for Unit C3a–b and at Take-shima for Unit C3c). Here, we used an exponential decay model, which is often used for estimating the volume of fallout deposits (e.g. Pyle, 1989) or ignimbrites (e.g. Wilson, 1991). In the exponential decay model, the thickness (T) of deposit can be written as $T = T_{\max} e^{bx}$ where $T_{\max}$ is the maximum thickness, b is the constant, and x is the distance from a location where the thickness is maximum. And the volume of product (V) can be written as $V = 2T_{\max}\pi / b^2$ $(0 < x < \infty)$. An approximation curve for the thickness–distance plot of Unit C3a–b using $T_{\max}$ 4 m is shown as a line 1 in Fig. 8c, and the volume is estimated to be about 10 km^3. On the other hand, a best-fit approximation curve (line 2 in Fig. 8c) yields $T_{\max}$ 3 m, and the volume is estimated to be about 8 km^3. The thickness of Unit C3c has a maximum in slight distal area (Take-shima). Therefore, assuming the linear increase of thickness in proximal area, we modified the volume equation as $V = 2\pi x_0^2 T_{\max} / 3 (0 < x < x_0) + 2T_{\max}\pi / b^2 (x_0 < x < \infty)$. Assuming x_0 and $T_{\max}$ to be 15 km and 30 m, respectively, an approximation curve for the thickness–distance plot of Unit C3c is shown as a line 1 in Fig. 8d, and the volume is estimated to be 30–35 km^3. On the other hand, a best-fit approximation curve (line 2 in Fig. 8d) yields

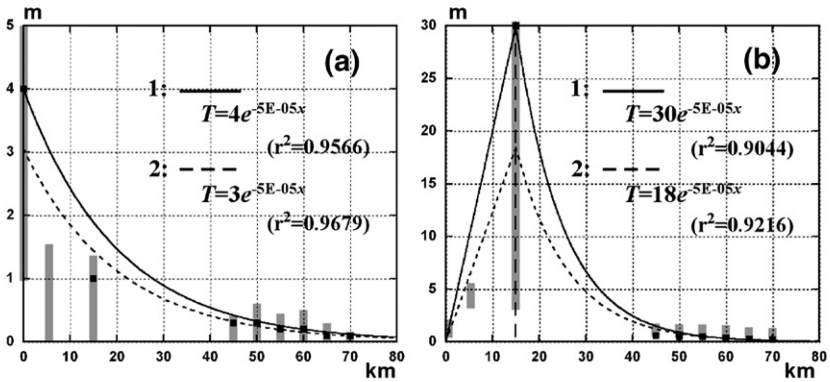

Fig. A1. Range and average values for the thickness of (a) Units C3a–b and (b) Unit C3c on proximal and distal areas. Assuming the deposit thickness (T) exponentially decaying with distance (x) from the maximum one (T_{max}), (a–1) an approximation curve using T_{max} 4 m and (a–2) a best-fit approximation curve for the thickness–distance plot of Unit C3a–b, and (b–1) an approximation curve using T_{max} 30 m and (b–2) a best-fit approximation curve for the thickness–distance plot of Unit C3c where the linear increase of thickness is assumed in proximal area.

T_{max} 18 m, and the volume is estimated to be 20–25 km^3. As a result, the volumes of Unit C3a–b and Unit C3c were roughly estimated to be about 10 km^3 and 20–35 km^3, respectively. The total volume of ignimbrite is assumed to be 30–45 km^3 (15–25 km^3 in total DRE, assuming deposit-density 1.5–2 g/cm^3 for Unit C3a–b and 1–1.2 g/ cm^3 for Unit C3c).

References

Allen, S.R., Cas, R.A.F., 1998. Rhyolitic fallout and pyroclastic density current deposits from a phreatoplinian eruption in the eastern Aegean Sea, Greece. J. Volcanol. Geotherm. Res. 86, 219–251.

Allen, S.R., Cas, R.A.F., 2001. Transport of pyroclastic flows across the sea during the explosive, rhyolitic eruption of the Kos Plateou Tuff, Greece. Bull. Volcanol. 62, 441–456.

Allen, S.R., Stewart, A.L., 2003. Products of explosive subaqueous felsic eruptions based on examples from the Hellenic Island Arc, Greece. In: White, D.L., Smellie, J.L., Clague, D.A. (Eds.), Explosive subaqueous volcanism, vol. 140. AGU Geophysical Monograph, pp. 285–298.

Aramaki, S., 1984. Formation of the Aira caldera, Southern Kyushu, 22,000 years ago. J. Geophys. Res. 89, 8485–8501.

Belousov, A., 1996. Deposits of the 30 March 1956 directed blast at Bezyminanny volcano, Kamchatka, Russia. Bull. Volcanol. 57, 649–662.

Bower, S.M., Woods, A.W., 1997. Control of magma volatile content and chamber depth on the mass erupted during explosive volcanic eruptions. J. Geophys. Res. 102, 10273–10290.

Branney, M.J., Kokelaar, P., 2002. Pyroclastic density currents and the sedimentation of ignimbrites. Geol. Soc. Lond. Mem. 27 (143 pp.).

Brown, R.J., Branney, M.J., 2004. Event-stratigraphy of a caldera-forming ignimbrite eruption on Tenerife: the 273 ka Poris Formation. Bull. Volcanol. 66, 392–416.

Carey, S., Sparks, R.S.J., 1986. Quantitative models of the fallout and dispersal of tephra from volcanic eruption columns. Bull. Volcanol. 48, 109–125.

Carey, S., Sigurdsson, H., 1989. The intensity of plinian eruption. Bull. Volcanol. 51, 28–40.

Carey, S., Sigurdsson, H., Mandeville, C., Bronto, S., 1996. Pyroclastic flows and surges over water: an example from the 1883 Krakatau eruption. Bull. Volcanol. 57, 493–511.

Carey, S., Sigurdsson, H., Mandeville, C., Bronto, S., 2000. Volcanic hazards from pyroclastic flow discharge into the sea: examples from 1883 eruption of Krakatau, Indonesia. Geol. Soc. Am., Spec. Pap. 345, 1–14.

Cas, R.AF., Wright, J.V., 1991. Subaqueous pyroclastic flows and ignimbrites: an assessment. Bull. Volcanol. 53, 357–380.

Dobran, F., Papale, P., 1993. Magma–water interaction in closed systems and application to lava tunnels and volcanic conduits. J. Geophys. Res. 98 (B8), 14041–14058.

Druitt, T.H., Bacon, C.R., 1986. Lithic breccia and ignimbrite erupted during the collapse of Crater Lake caldera, Oregon. J. Volcanol. Geotherm. Res. 29, 1–32.

Druitt, T.H., Sparks, R.S.J., 1984. On the formation of calderas during ignimbrite eruption. Nature 310, 679–681.

Fisher, R.V., 1990. Transport and deposition of a pyroclastic surge across an area of high relief: the 18 May 1980 eruption of Mount St. Helens, Washington. Geol. Soc. Am. Bull. 102, 1038–1054.

Fisher, R.V., Orsi, G., Ort, M., Heiken, G., 1993. Mobility of a large-volume pyroclastic flow-emplacement of the Campanian ignimbrite, Italy. J. Volcanol. Geotherm. Res. 56, 205–220.

Freundt, A., Bursik, M.I., 1998. Pyroclastic transport mechanisms. In: Freundt, A., Rosi, M. (Eds.), From Magma to Tephra. Elsevier Science. 276 pp.

Freundt, A., Schmincke, H., 1985. Lithic-enriched segregation bodies in pyroclastic flow deposits of Laacher See volcano (East Eifel, Germaney). J. Volcanol. Geotherm. Res. 25, 193–224.

Heiken, G., McCoy, F.W., 1984. Caldera development during the Minoan eruption, Thira, Cyclades, Greece. J. Geophys. Res. 89 (B10), 8441–8462.

Kawanabe, Y., Saito, G., 2002. Volcanic activity of the Satsuma–Iwojima area during the past 6500 years. Earth Planets Space 54, 295–301.

Kobayashi, T., Hayakawa, Y., 1984. Geology of Kikai caldera (Source of the Koya Ignimbrite), Japan. A progress report of the U.S.-Japan Cooperative Science Program, pp. 13–14.

Koyaguchi, T., Woods, A.W., 1996. On the formation of eruption columns following explosive mixing of magma and surface-water. J. Geophys. Res. 101, 5561–5574.

LaCroix, A., 1904. La Montagne Pelée et ses eruptions. Masson, Paris. 653 pp.

Legros, F., Kelfoun, K., Marti, J., 2000. The influence of conduit geometry on the dynamics of caldera-forming eruptions. Earth Planet. Sci. Lett. 179, 53–61.

Macedonio, G., Dobran, F., Neri, A., 1994. Erosion processes in volcanic conduits and application to the AD 79 eruption of Vesuvius. Earth Planet. Sci. Lett. 121, 137–152.

Machida, H., Arai, F., 1978. Akahoya ash — a Holocene widespread tephra erupted from the Kikai Caldera, South Kyusyu, Japan. Quat. Res. (Daiyonki–Kienkyu) 17, 143–163 (in Japanese with English abstract).

Machida, H., Arai, F., 2003. Atlas of Tephra in and around Japan. University of Tokyo Press. 336 pp. (in Japanese).

Machida, H., Ōta, Kawana, T., Moriwaki, H., Nagaoka, S., 2001. Geomorphology of Japan 7 Kyushu–Nansei syotou. University of Tokyo Press. 355 pp. (in Japanese).

Maeno, F., Taniguchi, H., 2005. Eruptive history of Satsuma Iwo-jima Island, Kikai, caldera, after a 6.5 ka caldera-forming eruption. Bull. Volcanol. Soc. Jpn. Ser. 2 (50), 71–85 (in Japanese with English abstract).

Maeno, F., Taniguchi, H., 2006. Silicic lava dome growth in the 1934–1935 Showa Iwo-jima eruption, Kikai caldera, south of Kyushu, Japan. Bull. Volcanol. 68, 673–688.

Maeno, F., Imamura, F., Taniguchi, H., 2006. Numerical simulation of tsunami generated by caldera collapse during the 7.3 ka Kikai eruption, Japan. Earth Planets Space 58, 1013–1024.

Marti, J., Folch, A., Neri, A., Macedonio, G., 2000. Pressure evolution during explosive caldera-forming eruptions. Earth Planet. Sci. Lett. 175, 275–287.

McCoy, F.W., Heiken, G., 2000. The Late-Bronze age explosive eruption of Thera (Santorini), Greece: regional and local effects. Geol. Soc. Am., Spec. Pap. 345, 43–70.

Naruo, H., Kobayashi, T., 2002. Two large-earthquakes triggered by a 6.5 ka BP eruption from Kikai caldera, southern Kyushu, Japan. Quat. Res. (Daiyonki–Kienkyu) 41, 287–299 (in Japanese with English abstract).

Newhall, C.G, Self, S., 1982. The volcanic explosivity index (VEI) — an estimate of explosive magnitude for historical volcanism. J. Geophys. Res. 87, 1231–1238.

Okuno, M., Fukushima, D., Kobayashi, T., 2000. Tephrochronology in Southern Kyushu, SW Japan: tephra layers for the past 100,000 years. J. Soc. Hum. Hist. 12, 9–23.

Ono, K., Soya, T., Hosono, T., 1982. Geology of the Satsuma-Io-Jima District. Quadrangle Series, Scale 1:50000. Geol. Surv. Jpn. 1–80 (in Japanese with English abstract).

Ōki, K., 2002. Changes in depositional environments during the post-glacial stage in Kagoshima Bay and Seas around the Northern Part of the Ryukyu Islands. Quat. Res. (Daiyonki–Kienkyu) 41, 237–250 (in Japanese with English abstract).

Papale, P., Dobran, F., 1993. Modeling of the ascent of magma during the plinian eruption of Vesuvius in A.D. 79. J. Volcanol. Geotherm. Res. 58, 101–132.

Pyle, D.M., 1989. The thickness, volume and grainsize of tephra fall deposits. Bull. Volcanol. 51, 1–15.

Roche, O., Druitt, T.H., 2001. Onset of caldera collapse during ignimbrite eruptions. Earth Planet. Sci. Lett. 191, 191–202.

Roche, O., Druitt, T.H., Merle, O., 2000. Experimental study of caldera formation. J. Geophys. Res. 105 (B1), 395–416.

Rosi, M., Pladio-Melosantos, M.L., Di Muro, A., Leoni, R., Bacolcol, T., 2001. Fall vs flow activity during the 1991 climactic eruption of Pinatubo Volcano (Philippines). Bull. Volcanol. 62, 549–566.

Saito, G., Kazahaya, K., Shinohara, H., Stimac, J., Kawanabe, Y., 2001. Variation of volatile concentration in a magma system of Satsuma–Iwojima volcano deduced from melt inclusion analyses. J. Volcanol. Geotherm. Res. 108, 11–31.

Saito, G., Stimac, J., Kawanabe, Y., Goff, F., 2002. Mafic inclusions in rhyolites of Satsuma–Iwojima volcano: evidence for mafic–silicic magma interaction. Earth Planets Space 54, 303–325.

Saito, G., Kazahaya, K., Shinohara, H., 2003. Volatile evolution of Satsuma–Iwojima volcano: degassing process and mafic–felsic magma interaction. In: De Vivo, B., Bodnar, R.J. (Eds.), Melt inclusions in volcanic systems: methods, applications and problems. Developments in Volcanology, vol. 5. Elsevier Science, pp. 129–146.

Scott, W.E., Hoblitt, R.P., Torres, R.C., Self, S., Martinez, M.L., Nillos, T.J., 1996. Pyroclastic flows of the June 15, 1991, climatic eruption of Mount Pinatubo. In: Newhall, C.G., Punongbayan, S. (Eds.), Fire and Mud: Eruptions of Mount Pinatubo, Philippines. Philippine Institute Volcanology and Seismology. Quezon City and University of Washington Press, Seattle, pp. 545–570.

Self, S., 1983. Large-scale phreatomagmatic silicic volcanism: a case study from New Zealand. J. Volcanol. Geotherm. Res. 17, 433–469.

Sigurdsson, H., Carey, S., Mandeville, C., Bronto, S., 1991. Pyroclastic flows of the 1883 Krakatau Eruption. Eos 72 (36), 377–392.

Simkin, T., Fiske, R.S., 1983. Krakatau 1883 — Eruption and its Effects. Smithsonian Institution Press, Washington D.C. 464 pp.

Sparks, R.S.J., Wilson, L., 1976. A model for the formation of ignimbrite by gravitational column collapse. J. Geol. Soc. (Lond.) 132, 441–451.

Sohn, Y.K., Chough, S.K., 1989. Depositional process of the Suwolbong tuff ring, Cheju Island (Korea). Sedimentology 36, 837–855.

Streck, M.J., Grunder, A.L., 1995. Crystallization and welding variations in a widespread ignimbrite sheet; the Rattlesnake tuff, eastern Oregon, USA. Bull. Volcanol. 57, 151–169.

Suzuki-Kamata, K., Kamata, H., 1990. The proximal facies of the Tosu pyroclastic-flow deposit erupted from Aso caldera, Japan. Bull. Volcanol. 52, 325–333.

Suzuki-Kamata, K., Kamata, H., Bacon, C.R., 1993. Evolution of the caldera-forming eruption at Crater Lake, Oregon, indicated by component analysis of lithic fragments. J. Geophys. Res. 98 (B8), 14059–14074.

Tanakadate, H., 1935. Evolution of a new volcanic islet near Io-zima (Satsuma Prov.). Proc. Imp. Acad. 11, 152–154.

Ui, T., 1973. Exceptionally far-reaching, thin pyroclastic flow in Southern Kyushu, Japan. Bull. Volcanol. Soc. Jpn. Ser. 2 (18), 153–168.

Ui, T., Metsugi, H., Suzuki, K., Walker, G.P.L., McBroome, L.A., Caress, M.E. (Eds.), 1984. Flow Lineation of Koya Low-aspect Ratio Ignimbrite, South Kyusyu, Japan. A progress report of the U.S.–Japan Cooperative Science Program, pp. 9–12.

Walker, G.P.L., 1983. Ignimbrite types and ignimbrite problems. J. Volcanol. Geotherm. Res. 17, 65–88.

Walker, G.P.L., 1985. Origin of coarse lithic breccias near ignimbrite source vents. J. Volcanol. Geotherm. Res. 25, 157–171.

Walker, G.P.L., Heming, R.F., Wilson, C.J.N., 1980. Low-aspect ratio ignimbrite. Nature 283, 286–287.

Walker, G.P.L., Self, S., Froggatt, P.C., 1981. The ground layer of the Taupo Ignimbrite: a striking example of sedimentation from a pyroclastic flow. J. Volcanol. Geotherm. Res. 10, 1–11.

Walker, G.P.L., McBroome, L.A., Caress, M.E. (Eds.), 1984. Products of the Koya Eruption from the Kikai Caldera, Japan. A progress report of the U.S.–Japan Cooperative Science Program, pp. 4–8.

Wilson, C.J.N., 1991. Ignimbrite morphology and the effects of erosion: a New Zealand case study. Bull. Volcanol. 53, 635–644.

Wilson, C.J.N., 2001. The 26.5 ka Oruanui eruption, New Zealand: introduction and overview. J. Volcanol. Geotherm. Res. 112, 133–174.

Wilson, C.J.N., Walker, G.P.L., 1985. The Taupo eruption, New-Zealand: I. General aspects. Philos. Trans. R. Soc. Lond. Ser. A: Math. Phys. Sci. 314, 229–310.

Wilson, L., Sparks, R.S.J., Walker, G.P.L., 1980. Explosive volcanic eruptions IV. The control of magma properties and conduit geometry on eruption column behavior. Geophys. J. R. Astron. Soc. 63, 117–148.

Wilson, C.J.N., Houghton, B.F., Kamp, P.J.J., McWilliams, M.O., 1995. An exceptionally widespread ignimbrite with implications for pyroclastic flow emplacement. Nature 378, 605–607.

Wohletz, K.H., 1998. Pyroclastic surges and compressible two-phase flow. In: Freundt, A., Rosi, M. (Eds.), From magma to tephra. Elsevier Science, pp. 247–312.

Woods, A.W., 1988. The fluid dynamics and thermodynamics of eruption columns. Bull. Volcanol. 50, 169–193.

Wright, I.C., Gamble, J.A., 1999. Southern Kermadec submarine caldera arc volcanoes (SW Pacific): caldera formation by effusion and pyroclastic eruption. Mar. Geol. 161, 207–227.

Yajima, K., Ono, M., Fujimaki, H., 2001. Analytical accuracy and precision of major and trace elements for bulk rocks using a 1:5 dilution glass bead by XRF. Jpn. Mag. Min. Petrol. Sci. 30, 28–32.

Yuasa, M., Murakami, F., Saito, E., Watanabe, K., 1991. Submarine topography of seamounts on the volcanic front of the Izu-Ogawara (Bonin) arc. Bull. Geol. Surv. Jpn. 42, 703–743.

Zheng, X., Zhang, W., Lizhong, Y., Endo, K., 1994. Paleoenvironmental changes in Southern Yangtze Delta over the Last 20,000 years. Quat. Res. 33, 379–384.